

RESEARCH ARTICLE

Open Access



Combination therapy for melanoma with BRAF/MEK inhibitor and immune checkpoint inhibitor: a mathematical model

Xiulan Lai^{1*} and Avner Friedman²

Abstract

Background: The B-raf gene is mutated in up to 66% of human malignant melanomas, and its protein product, BRAF kinase, is a key part of RAS-RAF-MEK-ERK (MAPK) pathway of cancer cell proliferation. BRAF-targeted therapy induces significant responses in the majority of patients, and the combination BRAF/MEK inhibitor enhances clinical efficacy, but the response to BRAF inhibitor and to BRAF/MEK inhibitor is short lived. On the other hand, treatment of melanoma with an immune checkpoint inhibitor, such as anti-PD-1, has lower response rate but the response is much more durable, lasting for years. For this reason, it was suggested that combination of BRAF/MEK and PD-1 inhibitors will significantly improve overall survival time.

Results: This paper develops a mathematical model to address the question of the correlation between BRAF/MEK inhibitor and PD-1 inhibitor in melanoma therapy. The model includes dendritic and cancer cells, CD4⁺ and CD8⁺ T cells, MDSC cells, interleukins IL-12, IL-2, IL-6, IL-10 and TGF- β , PD-1 and PD-L1, and the two drugs: BRAF/MEK inhibitor (with concentration γ_B) and PD-1 inhibitor (with concentration γ_A). The model is represented by a system of partial differential equations, and is used to develop an efficacy map for the combined concentrations (γ_B, γ_A). It is shown that the two drugs are positively correlated if γ_B and γ_A are at low doses, that is, the growth of the tumor volume decreases if either γ_B or γ_A is increased. On the other hand, the two drugs are antagonistic at some high doses, that is, there are zones of (γ_B, γ_A) where an increase in one of the two drugs will increase the tumor volume growth, rather than decrease it.

Conclusions: It will be important to identify, by animal experiments or by early clinical trials, the zones of (γ_B, γ_A) where antagonism occurs, in order to avoid these zones in more advanced clinical trials.

Keywords: Melanoma, Mathematical modeling, BRAF/MEK inhibitor, PD-1 inhibitor, Combination therapy

Background

PD-1 is an immunoinhibitory receptor predominantly expressed on activated T cells [1, 2]. Its ligand PD-L1 is upregulated on the same activated T cells, and is also expressed by myeloid-derived suppressor cells (MDSCs) [2–5] and in some human cancer cells, including melanoma, lung cancer, colon cancer, and leukemia [2, 3]. The complex PD-1-PD-L1 is known to inhibit T cell function [1]. Immune checkpoints are regulatory pathways in the immune system that inhibit its active response against

specific targets. In the case of cancer, the complex PD-1-PD-L1 functions as an immune checkpoint for anti-tumor T cells. There has been much progress in recent years in developing checkpoint inhibitors, primarily anti-PD-1 and anti-PD-L1 [6].

The B-raf gene is mutated in up to 66% of human malignant melanomas, and its protein product, BRAF kinase, is a key part of the RAS-RAF-MEK-ERK (MAPK) pathway of cancer cell proliferation [7]. BRAF-targeted therapy induces significant response in the majority of patients but the response is short lived (about 6 months) [7–9]. Initial clinical trials indicate that concurrent inhibition of BRAF with MEK decreases MAPK-driven acquired resistance,

*Correspondence: xiulanlai@ruc.edu.cn

¹Institute for Mathematical Sciences, Renmin University of China, 100872 Beijing, People's Republic of China

Full list of author information is available at the end of the article

resulting in enhanced clinical efficacy and decreased toxicity [10, 11]. This provides a rationale for using combined BRAF/MEK inhibition instead of BRAF inhibition alone [11]. Treatment of melanoma with immune checkpoint inhibitors has a lower response rate compared to treatment with BRAF/MEK inhibitors, but the response tends to be more durable, lasting for years [11–13]. It was therefore suggested that BRAF/MEK-targeted therapy may synergize with the PD-1 pathway blockade to enhance anti-tumor immunity [4, 11, 14, 15]. Meta-Analysis of randomized clinical trials show that compared with other treatments of advanced BRAF-mutated melanoma, combined BRAF/MEK and PD-1 inhibitions significantly improved overall survival time [16].

In this paper we develop a mathematical model to address the efficacy of the combination of BRAF/MEK inhibitor (BRAF/MEKi) and anti-PD-1 (e.g. nivolumab). The model includes several types of T cells, MDSCs, and dendritic cells, as well as signaling molecules involved in the crosstalks among these cells.

Melanoma-derived factors alter the maturation and activation of tissue-resident dendritic cells, thus favoring tumor immune escape [17]. In BRAF mutant melanoma, BRAF inhibitor restores the compromised dendritic cells function, and, in particular, the production of IL-12 by dendritic cells [18]. Although MEK inhibitor (e.g. trametinib), as single agent, negatively impacts DC function, when combined with BRAF inhibitor (e.g. vemurafenib or dabrafenib), the functionality of DCs is restored, as well as their production of IL-12 [18, 19].

Dendritic cell-derived IL-12 activates effector T cells (Th1 and CD8⁺ T cells) [20, 21]. Th1 produces IL-2 which further promotes proliferation of effector T cells. CD4⁺ T cells (Th1) can kill cancer cell directly, for example, through FAS- or TRAIL-dependent pathway

[22–25], while CD8⁺ T cell is more effective in killing cancer cells [26]. Cancer cells suppress the functions of effector T cells by producing immunosuppressor cytokines TGF- β , IL-6, CCL2 and IL-10 [27]. IL-10 inhibits the activation of Th1 and CD8⁺ T cells [27]. IL-6 and CCL2 recruit MDSCs into tumor [19, 28, 29], and MDSCs produce TGF- β and IL-10. IL-6 and CCL2 also recruit T regulatory T cells (Tregs) [15, 28, 29]. TGF- β is produced not only by cancer cells and MDSCs, but also by Tregs [30], and Tregs become activated by TGF- β [30, 31]. Tregs modulate Th1 and CD8⁺ T cells [30], thus promoting tumor growth.

One of the checkpoints on T cells is the membrane protein PD-1. Its ligand PD-L1 is expressed on activated effector T cells, on MDSCs and on cancer cells [2–5]. The complex PD-1-PD-L1 inhibits the function of effector T cells [1], but enhances the activation of Tregs [32] and thus promoting cancer.

The above interactions between cancer cells and the immune cells are summarized in Fig. 1. The mathematical model developed in the present paper is based on Fig. 1, and it includes BRAF/MEK and PD-1 inhibitors. Simulations of the model show that at low doses the two drugs are positively correlated, in the sense that the tumor volume decreases as each of the drugs is increased. However, at high doses the two drugs may become antagonistic, that is, an increase in dose of one of the drugs may actually result in an increase in the tumor volume.

Methods

Mathematical model

The mathematical model is based on the network shown in Fig. 1. The list of variables is given in Table 1. Since CCL2 and IL-6 are both produced by cancer cells and both recruit MDSCs and Tregs into tumor environment, we

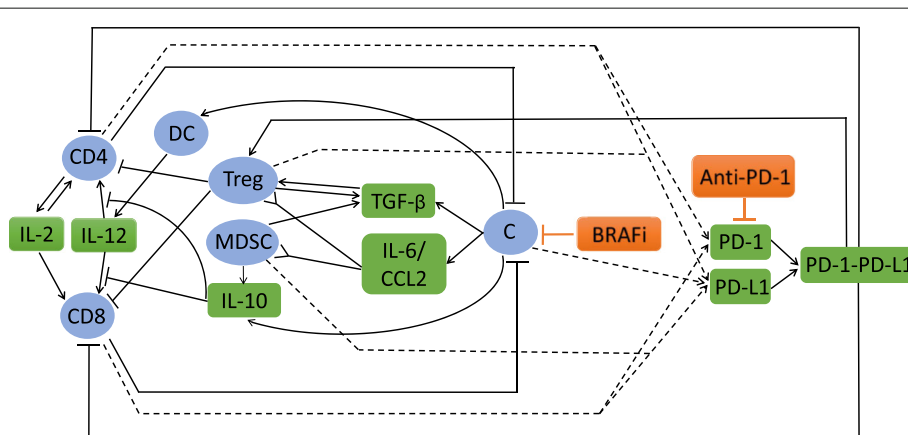


Fig. 1 Interaction of immune cells with cancer cells. Sharp arrows indicate proliferation/activation, blocked arrows indicate killing/blocking, inverted sharp arrows indicate recruitment/chemoattraction, and dashed lines indicate proteins on T cells, MDSCs and cancer cells

Table 1 List of variables (in units of g/cm³)

| Notation | Description |
|-----------|---|
| H | HMGB-1 concentration |
| N_C | Density of necrotic cancer cells |
| D | Density of DCs |
| T_1 | Density of activated CD4 ⁺ T cells |
| T_8 | Density of activated CD8 ⁺ T cells |
| T_r | Density of activated Treg cells |
| M | Density of activated MDSCs |
| C | Density of cancer cells |
| I_{12} | IL-12 concentration |
| I_2 | IL-2 concentration |
| T_β | TGF- β concentration |
| I_6 | IL-6 concentration |
| I_{10} | IL-10 concentration |
| P | PD-1 concentration |
| L | PD-L1 concentration |
| Q | PD-1-PD-L1 concentration |
| A | Anti-PD-1 concentration |
| B | BRAF/MEK inhibitor concentration |

shall consider, for simplicity, only IL-6 in our model.

We assume that the total density of cells within the tumor remains constant in space and time:

$$C + D + T_1 + T_8 + T_r + M = \text{constant}. \tag{1}$$

We assume that the density of debris of dead cells from necrosis or apoptosis is constant. We also assume that the densities of immature dendritic cells and naive CD4⁺ and CD8⁺ T cells remain constant throughout the tumor tissue. Under the assumption (1), proliferation of cancer cells and immigration of immune cells into the tumor, give rise to internal pressure which results in cells movement. We assume that all the cells move with the same velocity, \mathbf{u} ; \mathbf{u} depends on space and time and will be taken in unit of cm/day. We also assume that all the cells undergo dispersion (i.e., diffusion), and that all the cytokines and anti-tumor drugs are diffusing within the tumor.

Equation for DCs (D)

By necrotic cancer cells (N_C) we mean cancer cells undergoing the process of necrosis. Necrotic cancer cells release HMGB-1 (H) [33]. We model the dynamics of N_C and H by the following equations:

$$\frac{\partial N_C}{\partial t} + \underbrace{\nabla \cdot (\mathbf{u}N_C)}_{\text{velocity}} - \underbrace{\delta_{N_C} \nabla^2 N_C}_{\text{diffusion}} = \underbrace{\lambda_{N_C} C}_{\text{derived from alive cancer cells}} - d_{N_C} N_C,$$

$$\frac{\partial H}{\partial t} - \underbrace{\delta_H \nabla^2 H}_{\text{diffusion}} = \underbrace{\lambda_{HN_C} N_C}_{\text{released from necrotic cancer cells}} - \underbrace{d_H H}_{\text{degradation}},$$

where λ_{N_C} is the rate at which cancer cells become necrotic, d_N is the rate at which necrotic cells turn into debris, and λ_{HN_C} is the rate at which necrotic cells produce HMGB-1. We note that although molecules like HMGB-1, or other proteins, may be affected by the velocity \mathbf{u} , their diffusion coefficients are several order of magnitude larger than the diffusion coefficients of cells, hence their velocity term may be neglected. The degradation of HMGB-1 is fast ($\sim 0.01/\text{day}$) [34], and we assume that the process of necrosis is also fast. We may then approximate the two dynamical equations by the steady state $\lambda_{N_C} C - d_{N_C} N_C = 0$ and $\lambda_{HN_C} N_C - d_H H = 0$, so that H is proportional to C .

Dendritic cells are activated by HMGB-1 [35, 36]. Hence, the activation rate of immature dendritic cells, with density D_0 , is proportional to $D_0 \frac{H}{K_H + H}$, or to $D_0 \frac{C}{K_C + C}$, since H is proportional to C . Here, the Michaelis-Menten law is used to account for the limited rate of receptor recycling time which takes place in the process of DCs activation. Hence, the dynamics of DCs is given by

$$\frac{\partial D}{\partial t} + \underbrace{\nabla \cdot (\mathbf{u}D)}_{\text{velocity}} - \underbrace{\delta_D \nabla^2 D}_{\text{diffusion}} = \underbrace{\lambda_{DC} D_0 \frac{C}{K_C + C}}_{\text{activation by HMGB-1}} - \underbrace{d_D D}_{\text{death}} \tag{2}$$

where δ_D is the diffusion coefficient and d_D is the death rate of DCs.

Equation for CD4⁺ T cells (T_1)

Naive CD4⁺ T cells differentiate into Th1 cells (T_1) under IL-12 (I_{12}) environment [20, 21], while IL-10 and Tregs inhibit the differentiation of naive CD4⁺ T cells into T_1 cells [27, 30]. The proliferation of activated T_1 cells is enhanced by IL-2. Both processes of activation and proliferation of T_1 are assumed to be inhibited by PD-1-PD-L1 (Q) by a factor $\frac{1}{1+Q/K_{TQ}}$. Hence T_1 satisfies the following equation:

$$\frac{\partial T_1}{\partial t} + \nabla \cdot (\mathbf{u}T_1) - \delta_T \nabla^2 T_1 = \left(\underbrace{\lambda_{T_1 I_{12}} T_{10} \cdot \frac{I_{12}}{K_{I_{12}} + I_{12}}}_{\text{activation by IL-12}} \cdot \underbrace{\frac{1}{1 + I_{10}/K_{T I_{10}}}}_{\text{inhibition by IL-10}} \right) \times \underbrace{\frac{1}{1 + T_r/K_{T T_r}}}_{\text{inhibition by Tregs}} + \underbrace{\lambda_{T_1 I_2} T_1 \frac{I_2}{K_{I_2} + I_2}}_{\text{IL-2-induced proliferation}} \times \underbrace{\frac{1}{1 + Q/K_{TQ}}}_{\text{inhibition by PD-1-PD-L1}} - d_{T_1} T_1, \tag{3}$$

where T_{10} is the density of the naive CD4⁺ T cells.

Equation for activated CD8⁺ T cells (T_8)

Inactive CD8⁺ T cells are activated by IL-12 [20, 21], and this process is resisted by IL-10 and Tregs [27, 30]. IL-2 enhances the proliferation of activated CD8⁺ T cells. Similarly to the equation for T_1 , T_8 satisfies the following equation:

$$\begin{aligned} \frac{\partial T_8}{\partial t} + \nabla \cdot (\mathbf{u}T_8) - \delta_T \nabla^2 T_8 = & \underbrace{\left(\lambda_{T_8 I_{12}} T_{80} \cdot \frac{I_{12}}{K_{I_{12}} + I_{12}} \right)}_{\text{activation by IL-12}} \\ & \times \underbrace{\frac{1}{1 + I_{10}/K_{TI_{10}}}}_{\text{inhibition by IL-10}} \cdot \underbrace{\frac{1}{1 + T_r/K_{TT_r}}}_{\text{inhibition by Tregs}} \\ & + \underbrace{\lambda_{T_8 I_2} T_8 \frac{I_2}{K_{I_2} + I_2}}_{\text{IL-2-induced proliferation}} \\ & \times \underbrace{\frac{1}{1 + Q/K_{TQ}}}_{\text{inhibition by PD-1-PD-L1}} - \underbrace{d_{T_8} T_8}_{\text{death}} \end{aligned} \tag{4}$$

where T_{80} is the density of the inactive CD8⁺ T cells.

Equation for activated Tregs (T_r)

Naive CD4⁺ T cells differentiate into Tregs (T_r) under activation by Fox3+ transcription factor. The complex PD-1-PD-L1 enhances the expression of PTEN, which results in upregulation of Fox3+, and hence in increased production of Tregs [32]. The production of T_r is also enhanced by TGF- β (T_β) [30, 31]. The activated Tregs are recruited into tumor by tumor-derived immunosuppressive cytokine IL-6 (and CCL2)[15, 28, 29]. Representing this chemoattraction by $\nabla \cdot (\chi T_r \nabla I_6)$, we get the following equation for T_r :

$$\begin{aligned} \frac{\partial T_r}{\partial t} + \nabla \cdot (\mathbf{u}T_r) - \delta_T \nabla^2 T_r = & T_{10} \left(\underbrace{\lambda_{T_r T_\beta} \frac{T_\beta}{K_{T_\beta} + T_\beta}}_{\text{TGF-}\beta\text{-induced proliferation}} + \underbrace{\lambda_{T_r Q} \frac{Q}{K_Q + Q}}_{\text{promotion by PD-1-PD-L1}} \right) \\ & - \underbrace{\nabla \cdot (\chi T_r \nabla I_6)}_{\text{recruited by IL-6}} - \underbrace{d_{T_r} T_r}_{\text{death}} \end{aligned} \tag{5}$$

Equation for activated MDSCs (M)

Tumor recruits macrophages and “educates” them to become tumor-associated-macrophages (TAMs), which behave like MDSCs [37, 38]. MDSCs are also chemotactically attracted to the tumor microenvironment by IL-6 (and CCL2) [15, 19, 28, 29, 39]. As in [40], the Eq. of

MDSCs is taken to be the following form:

$$\begin{aligned} \frac{\partial M}{\partial t} + \nabla \cdot (\mathbf{u}M) - \delta_M \nabla^2 M = & \lambda_M (M_0 - M) \\ & \times \frac{I_6}{K_{I_6} + I_6} - \underbrace{\nabla \cdot (\chi M \nabla I_6)}_{\text{recruited by IL-6}} - \underbrace{d_M M}_{\text{death}} \end{aligned} \tag{6}$$

where M_0 is the source/influx of macrophages from the blood.

Equation for tumor cells (C)

Cancer cells are killed by T_1 and T_8 cells. We assume a logistic growth with carrying capacity (C_M) in order to account for competition for space among cancer cells. BRAF/MEK inhibitor (B), for example vemurafenib/dabrafenib, is used for treatment of advanced melanoma. Its mechanism of action involves selective inhibition of the mutated BRAF kinase that leads to reduced signaling through the aberrant RAS-RAF-MEK-ERK (MAPK) pathway. We assume that BRAF/MEK inhibitor suppresses the abnormal proliferation of tumor cells by a factor $\frac{1}{1+B/K_{CB}}$. Then, the equation for C takes the form:

$$\begin{aligned} \frac{\partial C}{\partial t} + \nabla \cdot (\mathbf{u}C) - \delta_C \nabla^2 C = & \underbrace{\lambda_C C \left(1 - \frac{C}{C_M} \right)}_{\text{proliferation}} \cdot \underbrace{\frac{1}{1 + B/K_{CB}}}_{\text{inhibition by BRAF/MEKi}} \\ & - \underbrace{(\eta_1 T_1 C + \eta_8 T_8 C)}_{\text{killing by T cells}} - \underbrace{d_C C}_{\text{death}} \end{aligned} \tag{7}$$

where η_1 and η_8 are the killing rates of cancer cells by T_1 and T_8 , and d_C is the natural death rate of cancer cells.

Equation for IL-12 (I_{12})

The proinflammatory cytokine IL-12 is secreted by activated DCs [20, 21], so that

$$\begin{aligned} \frac{\partial I_{12}}{\partial t} - \delta_{I_{12}} \nabla^2 I_{12} = & \underbrace{\lambda_{I_{12} D} D}_{\text{production by DCs}} - \underbrace{d_{I_{12}} I_{12}}_{\text{degradation}} \end{aligned}$$

The maturation and activation of dendritic cells is interrupted by melanoma cells, which means that the production rate coefficient $\lambda_{I_{12} D}$ is small. However, in BRAF mutant melanoma, BRAF inhibitor alone or in combination with MEK inhibitor, restores the compromised dendritic cells function, and in particular, the production of IL-12 by dendritic cells [18, 19], and the corresponding equation for I_{12} then takes the form:

$$\begin{aligned} \frac{\partial I_{12}}{\partial t} - \delta_{I_{12}} \nabla^2 I_{12} = & \underbrace{\lambda_{I_{12} D} D \cdot \left(1 + \lambda_{I_{12} B} \frac{B}{K_B + B} \right)}_{\text{production by DCs}} - \underbrace{d_{I_{12}} I_{12}}_{\text{degradation}} \end{aligned} \tag{8}$$

Equation for IL-2 (I_2)

IL-2 is produced by activated CD4⁺ T cells (T_1) [21]. Hence,

$$\frac{\partial I_2}{\partial t} - \delta_{I_2} \nabla^2 I_2 = \underbrace{\lambda_{I_2 T_1} T_1}_{\text{production by } T_1} - \underbrace{d_{I_2} I_2}_{\text{degradation}}. \quad (9)$$

Equation for TGF- β (T_β)

TGF- β is produced by tumor cells [27], MDSCs [31, 41, 42] and Tregs [30]:

$$\begin{aligned} \frac{\partial T_\beta}{\partial t} - \delta_{T_\beta} \nabla^2 T_\beta = & \underbrace{\lambda_{T_\beta C} C}_{\text{production by cancer cells}} + \underbrace{\lambda_{T_\beta T_r} T_r}_{\text{production by Tregs}} \\ & + \underbrace{\lambda_{T_\beta M} M}_{\text{production by MDSCs}} - \underbrace{d_{T_\beta} T_\beta}_{\text{degradation}}. \end{aligned} \quad (10)$$

Equation for IL-6 (I_6)

IL-6 is produced by cancer cells [15, 19, 28], so that

$$\frac{\partial I_6}{\partial t} - \delta_{I_6} \nabla^2 I_6 = \underbrace{\lambda_{I_6 C} C}_{\text{production by cancer cells}} - \underbrace{d_{I_6} I_6}_{\text{degradation}} \quad (11)$$

Equation for IL-10 (I_{10})

IL-10 is produced by cancer cells and MDSCs [27]. Hence it satisfies the following equation:

$$\begin{aligned} \frac{\partial I_{10}}{\partial t} - \delta_{I_{10}} \nabla^2 I_{10} = & \underbrace{\lambda_{I_{10} C} C}_{\text{production by cancer cells}} + \underbrace{\lambda_{I_{10} M} M}_{\text{production by MDSCs}} \\ & - \underbrace{d_{I_{10}} I_{10}}_{\text{degradation}}. \end{aligned} \quad (12)$$

Equation for PD-1 (P), PD-L1 (L) and PD-1-PD-L1 (Q)

PD-1 is expressed on the surface of activated CD4⁺ T cells, activated CD8⁺ T cells and Tregs. We assume that the number of PD-1 per cell is the same for T_1 and T_8 cells, but is smaller, by a factor ε_T , for T_r cells. If we denote by ρ_P the ratio between the mass of one PD-1 protein to the mass of one T cell, then

$$P = \rho_P(T_1 + T_8 + \varepsilon_T T_r).$$

The coefficient ρ_P is constant when no anti-PD-1 drug is administered. And in this case, to a change in $T = T_1 + T_8 + \varepsilon_T T_r$, given by $\frac{\partial T}{\partial t}$, there corresponds a change of P , given by $\rho_P \frac{\partial T}{\partial t}$. For the same reason, $\nabla \cdot (\mathbf{u}P) = \rho_P \nabla \cdot (\mathbf{u}T)$

and $\nabla^2 P = \rho_P \nabla^2 T$ when no anti-PD-1 drug is injected. Hence, P satisfies the equation

$$\begin{aligned} \frac{\partial P}{\partial t} + \nabla \cdot (\mathbf{u}P) - \delta_T \nabla^2 P = & \rho_P \left[\frac{\partial(T_1 + T_8 + \varepsilon_T T_r)}{\partial t} + \nabla \right. \\ & \times (\mathbf{u}(T_1 + T_8 + \varepsilon_T T_r)) \\ & \left. - \delta_T \nabla^2(T_1 + T_8 + \varepsilon_T T_r) \right]. \end{aligned}$$

Recalling Eqs. (3)-(5) for T_1 , T_8 and T_r , we get

$$\begin{aligned} \frac{\partial P}{\partial t} + \nabla \cdot (\mathbf{u}P) - \delta_T \nabla^2 P = & \rho_P \left[(\lambda_{T_1 I_{12}} T_{10} + \lambda_{T_8 I_{12}} T_{80}) \frac{I_{12}}{K_{I_{12}} + I_{12}} \cdot \frac{1}{1 + I_{10}/K_{TI_{10}}} \right. \\ & \times \frac{1}{1 + T_r/K_{TT_r}} + (\lambda_{T_1 I_2} T_1 + \lambda_{T_8 I_2} T_8) \frac{I_2}{K_{I_2} + I_2} \left. \right] \times \frac{1}{1 + Q/K_{TQ}} \\ & + \rho_P \varepsilon_T T_{10} \cdot \left(\lambda_{T_r T_\beta} \frac{T_\beta}{K_{T_\beta} + T_\beta} + \lambda_{T_r Q} \frac{Q}{K_Q + Q} \right) \\ & - \rho_P [(d_{T_1} T_1 + d_{T_8} T_8 + \varepsilon_T d_{T_r} T_r) + \varepsilon_T \delta_{TI_6} \nabla \cdot (T_r \nabla I_6)] \end{aligned}$$

When anti-PD-1 drug (A) is applied, PD-1 is depleted (or blocked) by A . In this case, the ratio $\frac{P}{T_1 + T_8 + \varepsilon_T T_r}$ may change. In order to include in the model both cases of with and without anti-PD-1, we replace ρ_P in the previous equation by $\frac{P}{T_1 + T_8 + \varepsilon_T T_r}$. Hence,

$$\begin{aligned} \frac{\partial P}{\partial t} + \nabla \cdot (\mathbf{u}P) - \delta_T \nabla^2 P = & \frac{P}{T_1 + T_8 + \varepsilon_T T_r} \left[(\lambda_{T_1 I_{12}} T_{10} + \lambda_{T_8 I_{12}} T_{80}) \frac{I_{12}}{K_{I_{12}} + I_{12}} \cdot \frac{1}{1 + I_{10}/K_{TI_{10}}} \right. \\ & \times \frac{1}{1 + T_r/K_{TT_r}} + (\lambda_{T_1 I_2} T_1 + \lambda_{T_8 I_2} T_8) \frac{I_2}{K_{I_2} + I_2} \left. \right] \times \frac{1}{1 + Q/K_{TQ}} \\ & + \frac{P}{T_1 + T_8 + \varepsilon_T T_r} \varepsilon_T T_{10} \cdot \left(\lambda_{T_r T_\beta} \frac{T_\beta}{K_{T_\beta} + T_\beta} + \lambda_{T_r Q} \frac{Q}{K_Q + Q} \right) \\ & - \frac{P}{T_1 + T_8 + \varepsilon_T T_r} [(d_{T_1} T_1 + d_{T_8} T_8 + \varepsilon_T d_{T_r} T_r) + \varepsilon_T \delta_{TI_6} \nabla \cdot (T_r \nabla I_6)] \\ & - \underbrace{\mu_{PA} P A}_{\text{depletion by anti-PD-1}}, \end{aligned} \quad (13)$$

where μ_{PA} is the depletion rate of PD-1 by anti-PD-1.

PD-L1 is expressed on the surface of activated CD4⁺ T cells, activated CD8⁺ T cells, MDSCs, and tumor cells. We assume that the number of PD-L1 per cell is the same for T_1 , T_8 and M cells, and denote the ratio between the mass of one PD-L1 protein to the mass of one cell by ρ_L . Then

$$L = \rho_L(T_1 + T_8 + \varepsilon_M M + \varepsilon_C C), \quad (14)$$

where ε_C depends on the specific type of tumor.

PD-L1 from T cells or cancer cells combines with PD-1 on the plasma membrane of T cells, thus forming a complex PD-1-PD-L1 (Q) on the T cells [2, 3]. Denoting the

association and disassociation rates of Q by α_{PL} and d_Q , respectively, we can write

$$P + L \xrightleftharpoons[d_Q]{\alpha_{PL}} Q.$$

The half-life of Q is less than 1 second (i.e. 1.16×10^{-5} day) [43], so that d_Q is very large. Hence we may approximate the dynamical equation for Q by the steady state equation, $\alpha_{PL}PL = d_QQ$, or

$$Q = \sigma PL, \tag{15}$$

where $\sigma = \alpha_{PL}/d_Q$.

Equation for anti-PD-1 (A)

We assume that anti-PD-1 is injected intradermally every three days for 30 days (as in mouse experiments [44]), providing a source $\hat{A}(t)$ of anti-PD-1:

$$\hat{A}(t) = \begin{cases} \gamma_A & \text{if } t \leq 30, \\ \gamma_A \times \frac{33-t}{3} & \text{if } 30 < t \leq 33, \\ 0 & \text{if } t > 33. \end{cases}$$

where γ_A is the effective level of the drug; although the level of the drug varies between injections, for simplicity we take it to be constant. The drug A is depleted in the process of blocking PD-1. Hence,

$$\frac{\partial A}{\partial t} - \delta_A \nabla^2 A = \hat{A}(t) - \underbrace{\mu_{PA}PA}_{\text{depletion through blocking PD-1}} - \underbrace{d_{AA}A}_{\text{degradation}}. \tag{16}$$

Equation for BRAF/MEK inhibitor (B)

We assume that the BRAF/MEK inhibitor is injected intradermally every days for 30 days, providing a source $\hat{B}(t)$ of BRAF/MEKi:

$$\hat{B}(t) = \begin{cases} \gamma_B & \text{if } t \leq 30, \\ \gamma_B \times \frac{33-t}{3} & \text{if } 30 < t \leq 33, \\ 0 & \text{if } t > 33. \end{cases}$$

Assuming that BRAF/MEKi is absorbed by C at a rate $\mu_{BC}C \frac{B}{K_B+B}$, we get the following equation for B :

$$\frac{\partial B}{\partial t} - \delta_B \nabla^2 B = \hat{B}(t) - \underbrace{\mu_{BC}C \frac{B}{K_B+B}}_{\text{absorption by cancer cells}} - \underbrace{d_{BB}B}_{\text{degradation}}. \tag{17}$$

Equation for cells velocity (u)

We assume that a part of the tumor consists of extracellular matrix, ECM (approximately, 0.4 g/cm^3), cancer cells (approximately, $C = 0.4 \text{ g/cm}^3$) and MDSCs (approximately, $M = 0.2 \text{ g/cm}^3$). We assume (in the section of parameter estimation) that the densities of the immune cells D , T_1 , T_8 and T_r are approximately 4×10^{-4} , 2×10^{-3} , $1 \times 10^{-3} \text{ g/cm}^3$ and $5 \times 10^{-4} \text{ g/cm}^3$, respectively, and, for consistency, take the constant in Eq. (1) to be 0.6039. We

further assume that all cells have approximately the same volume and surface area, so that the diffusion coefficients of all the cells are the same. Adding Eqs. (2)-(7), we then get

$$0.6039 \times \nabla \cdot \mathbf{u} = \sum_{j=2}^7 [\text{RHS of Eq. (j)}]. \tag{18}$$

To simplify the computations, we assume that the tumor is spherical and denote its radius by $r = R(t)$. We also assume that all the densities and concentrations are radially symmetric, that is, functions of (r, t) , where $0 \leq r \leq R(t)$. In particular, $\mathbf{u} = u(r, t)\mathbf{e}_r$, where \mathbf{e}_r is the unit radial vector.

Equation for free boundary (R)

We assume that the free boundary $r = R(t)$ moves with the velocity of cells, so that

$$\frac{dR(t)}{dt} = u(R(t), t). \tag{19}$$

Boundary conditions

We assume that the naive $CD4^+$ T cells and inactive $CD8^+$ T cells that migrated from the lymph nodes into the tumor microenvironment have constant densities \hat{T}_1 and \hat{T}_8 at the tumor boundary, and that T_1 and T_8 are activated by IL-12 upon entering the tumor. We then have the following flux conditions at the tumor boundary:

$$\begin{aligned} \frac{\partial T_1}{\partial r} + \sigma_T(I_{12})(T_1 - \hat{T}_1) &= 0, \\ \frac{\partial T_8}{\partial r} + \sigma_T(I_{12})(T_8 - \hat{T}_8) &= 0 \text{ at } r = R(t), \end{aligned} \tag{20}$$

where $\sigma_T(I_{12}) = \sigma_0 \frac{I_{12}}{I_{12} + K_{I_{12}}}$.

We impose a no-flux boundary condition for all the remaining variables:

No-flux for D , T_r , M , C , I_{12} , I_2 , T_β , I_6 , I_{10} , P , A , and B at $r = R(t)$. (21)

It is tacitly assumed here that the receptors PD-1 and ligands PD-L1 become active only after the T cells are already inside the tumor.

Initial conditions

Later on we shall compare the simulations of the model with experimental results for mice, for 60 days. Accordingly, we take initial values whereby the average density of cancer cells has not yet increased to its steady state. Then, by Eq. (1), the total density of the immune cells is initially above its steady state. We take (in unit of g/cm^3):

$$\begin{aligned} D &= 2 \times 10^{-4}, T_1 = 4 \times 10^{-3}, T_8 = 2 \times 10^{-3}, \\ T_r &= 3 \times 10^{-3}, M = 0.22, C = 0.3774. \end{aligned} \tag{22}$$

Note that the initial conditions for the cells satisfy Eq. (1).

We assume that initially $B = 0$ and $A = 0$, and take the initial condition for I_{12} , I_2 , T_β , I_6 , I_{10} and P to be close to their steady state values, which are computed in the section on parameter estimation. One choice of initial conditions is given as follows (in unit of g/cm^3):

$$I_{12} = 4 \times 10^{-10}, I_2 = 4.74 \times 10^{-11}, T_\beta = 2.62 \times 10^{-13}, I_6 = 3.06 \times 10^{-11}, I_{10} = 9.66 \times 10^{-11}, P = 8.3 \times 10^{-10}.$$

However, other choices of these initial conditions do not affect the simulations of the model after a few days.

Results and discussions

The simulations of the model were performed by Matlab based on the moving mesh method for solving partial differential equations with free boundary [45] (see the section on computational method).

Figure 2 is a simulation of the model with no drugs (the control case) for the first 60 days. The average density or concentration of a species is computed as its total mass in the tumor divided by the tumor volume. The simulation shows consistency in the choice of the model parameters. Indeed, as can be quickly checked, the steady states of all the cytokines and cells are approximately equal to the half-saturation values that we assumed in estimating the parameters of the model. Furthermore, the volume of the tumor doubles approximately every 10 days, as was assumed in the choice of the parameter λ_0 (used in estimating some parameters of Eq. (7)). It is interesting to note that the initial increase in TGF- β more than compensates

for the initial decrease in P and L , as evident by the initial increase in T_r . This initial increase of T_r results in initial decrease in the T_1 and T_8 cells. We also note that the initial increase in cancer cells results in an increase in the D cells.

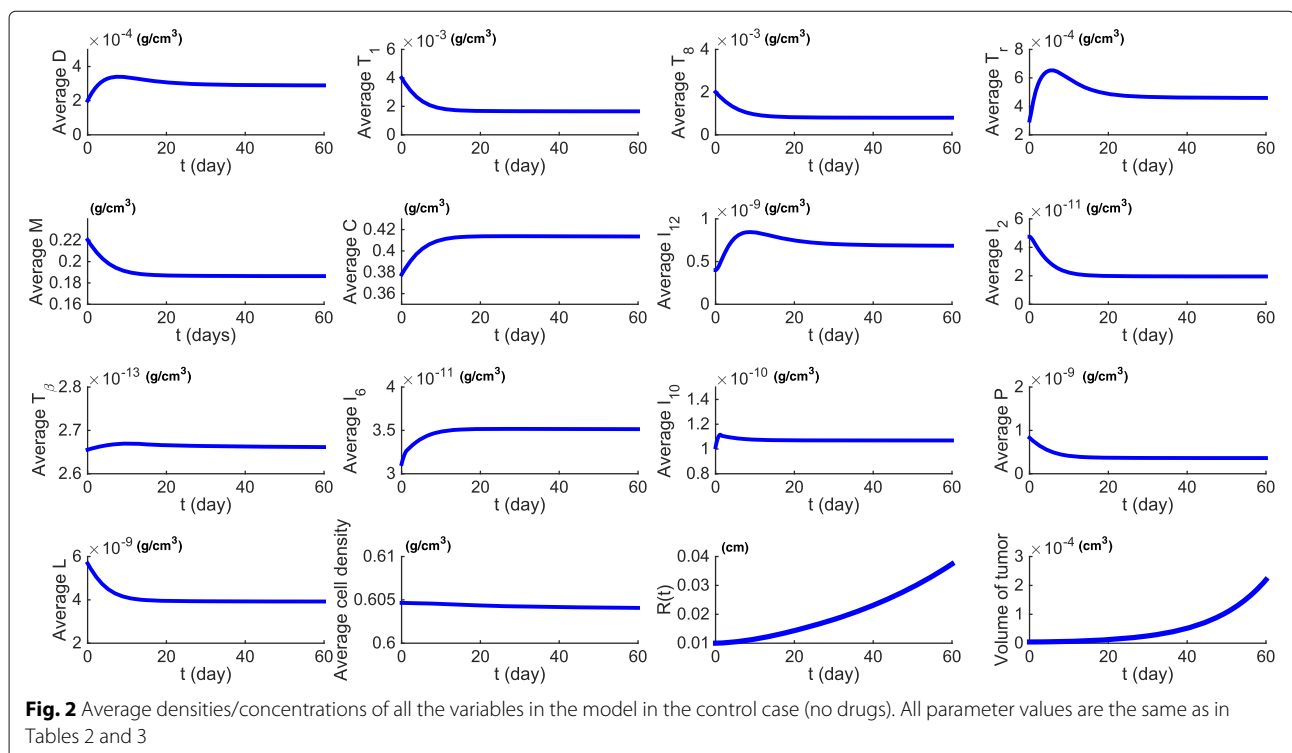
Figure 3 shows the growth of the tumor radius during 60 days when drug is administered. With no drugs, the radius increases from 0.01 cm to 0.037 cm. Treatment with BRAF/MEK inhibitor alone decreased the radius growth more than anti-PD-1 alone, and the combined therapy did better than anti-PD-1 alone. These results agree with mouse experiments reported in [44].

We next consider combination therapy for a range of values of BRAF/MEK inhibitor and anti-PD-1. We define the efficacy of a combination therapy, with (γ_B, γ_A) , by the formula:

$$E(\gamma_B, \gamma_A) = \frac{R_{60}(0, 0) - R_{60}(\gamma_B, \gamma_A)}{R_{60}(0, 0)},$$

where the tumor radius $R_{60} = R_{60}(\gamma_B, \gamma_A)$ is computed at day 60; $R_{60}(0, 0)$ is the radius at day 60 in the control case (no drugs). The efficacy is a positive number, and its value lies between 0 and 1 (or between 0 and 100%). Figure 4 is the efficacy map of the combined therapy, with γ_B in the range of $0 - 5 \times 10^{-9} \text{ g}/\text{cm}^3 \cdot \text{day}$ and γ_A in the range of $0 - 1.4 \times 10^{-9} \text{ g}/\text{cm}^3 \cdot \text{day}$. The color column shows the efficacy for any pair of (γ_B, γ_A) ; the maximum efficacy is 0.97 (97%).

As the number of cancer cells increases, the tumor radius increases. Hence, if T_1 and T_8 were monotone



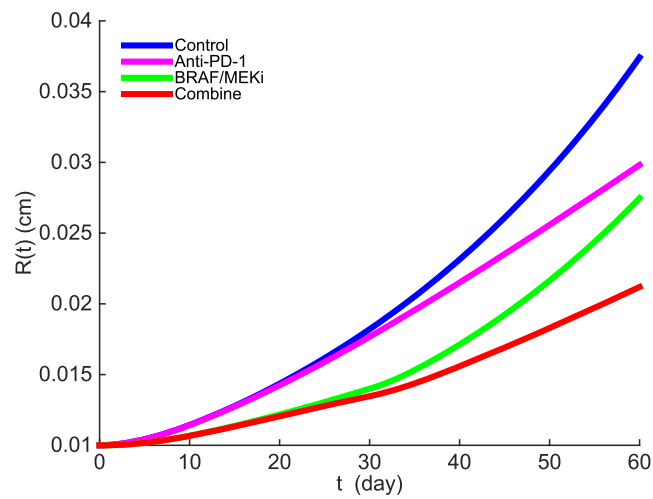


Fig. 3 The growth of tumor radius $R(t)$ during the administration of anti-PD-1 drug and BRAF/MEK inhibitors. Anti-PD-1 is administered at rate $\gamma_A = 0.3 \times 10^{-9} \text{ g/cm}^3 \cdot \text{day}$ and BRAF/MEK inhibitor is administered at rate $\gamma_B = 0.5 \times 10^{-9} \text{ g/cm}^3 \cdot \text{day}$. All other parameter values are the same as in Tables 2 and 3

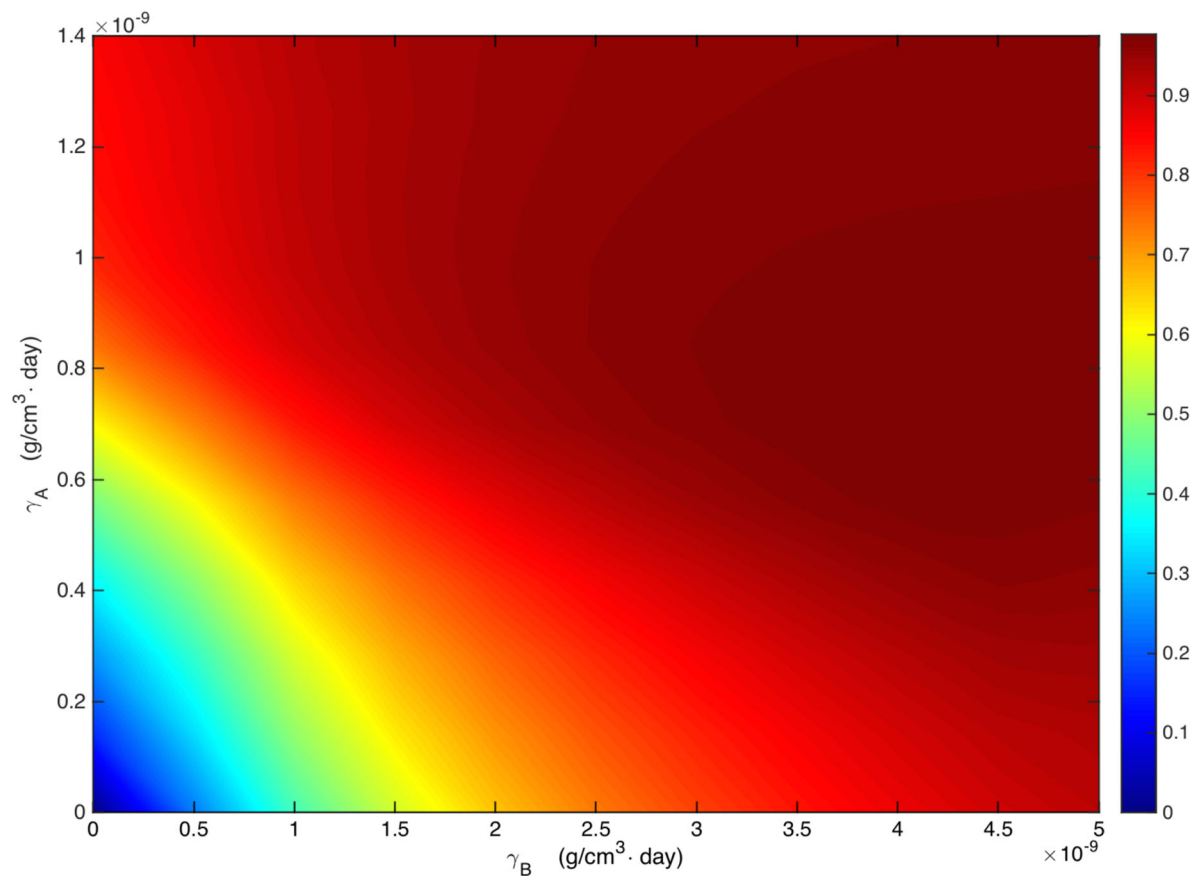


Fig. 4 Drug efficacy map. The color column shows the efficacy $E(\gamma_B, \gamma_A)$ when γ_B varies between $0 - 5 \times 10^{-9} \text{ g/cm}^3 \cdot \text{day}$ and γ_A varies between $0 - 1.4 \times 10^{-9} \text{ g/cm}^3 \cdot \text{day}$. All other parameter values are the same as in Tables 2 and 3

increasing functions of γ_A (or of γ_B), then we should see that $R_{60}(\gamma_B, \gamma_A)$ is a decreasing function of γ_A (or of γ_B), and $E(\gamma_B, \gamma_A)$ would then also be an increasing function of γ_A (or of γ_B). But Fig. 4 shows that this is not generally the case; indeed there are small oscillations in “northeast” corner of the figure. This means that the functions T_1 and T_8 cannot be monotone increasing with respect to γ_B for fixed $\gamma_A > 0.5 \times 10^{-9} \text{ g/cm}^3 \cdot \text{day}$, and also cannot be monotone increasing in γ_A for fixed $\gamma_B > 1.5 \times 10^{-9} \text{ g/cm}^3 \cdot \text{day}$. Indeed, for example, Fig. 5a shows that the average densities of T_1 and T_8 are decreasing functions of γ_B , for fixed $\gamma_A = 1.26 \times 10^{-9} \text{ g/cm}^3 \cdot \text{day}$; however, for smaller values of γ_A , T_1 and T_8 may become monotone increasing, as seen, for example, in Fig. 5b with $\gamma_A = 0.14 \times 10^{-9} \text{ g/cm}^3 \cdot \text{day}$. Similarly, Fig. 6a shows that, for fixed $\gamma_B = 3 \times 10^{-9} \text{ g/cm}^3 \cdot \text{day}$, there is a γ_A -interval where T_1 and T_8 are decreasing as γ_A increases. The γ_A -interval where T_1 and T_8 are decreasing may shrink as we take a smaller fixed γ_B , as seen, for example, in Fig. 6b with $\gamma_B = 0.1 \times 10^{-9} \text{ g/cm}^3 \cdot \text{day}$.

A possible explanation for Fig. 5a is based on the antagonistic pathway shown in Fig. 7. When γ_B increases, the population of cancer cells decreases, and then, by Eqs. (2)-(4) and (8), so does the signal to activate T cells by dendritic cells-derived IL-12 (since the number of activated dendritic cells decrease with decreased cancer cell density) and thus the densities of T_1 and T_8 decrease. As for Fig. 6a, when γ_A begins to increase, T_1 and T_8 also begin to increase, which results in a decrease of cancer cells. Then, as explained in the case of Fig. 5a, this leads to a decrease in dendritic cells-derived IL-12 and, hence, the density of activated T_1 and T_8 cells will begin to decrease as γ_A continues to increase for a while.

If we inject IL-12 directly into tumor (as an additional drug), the influence of dendritic cells-secreted IL-12 diminishes, and the antagonism between BRAF/MEKi and anti-PD-1 also diminishes and it disappears already at very small amount of injection, e.g., an injection of order of magnitude $10^{-14} \text{ gcm}^3 \cdot \text{day}$.

Sensitivity analysis

We performed sensitivity analysis, with respect to the tumor radius R at day 60 in the control case, with respect to some of the production parameters of the system (2)-(16), namely, λ_{DC} , $\lambda_{T_1 I_{12}}$, $\lambda_{T_8 I_{12}}$, $\lambda_{T_r T_\beta}$, $\lambda_{T_\beta C}$, $\lambda_{I_6 C}$, $\lambda_{I_{10} C}$, and the parameters K_{TQ} , η_1 and η_8 which play important role in the dynamics of C . Following the method of [46], we performed Latin hypercube sampling and generated 1000 samples to calculate the partial rank correlation coefficients (PRCC) and the p -values with respect to the tumor radius at day 60. In sampling all the parameters, we took the range of each from 1/2 to twice its values in Tables 2 and 3. The results are shown in Fig. 8.

We see that the production/activation rates that promote effector T cells, namely, λ_{DC} , $\lambda_{T_1 I_{12}}$ and $\lambda_{T_8 I_{12}}$, are negatively correlated to the tumor radius, while the production/activation rates of the effector T cell-suppressors, such as $\lambda_{T_r T_\beta}$, $\lambda_{I_{10} C}$, $\lambda_{T_\beta C}$ and $\lambda_{I_6 C}$, are positively correlated to the tumor radius. The killing rate of effector T cells, η_1 and η_8 are negatively correlated to the tumor radius, and the correlation with η_8 is higher than with η_1 .

Conclusion

BRAF mutation occurs in up to 66% of human malignant melanomas and for this reason BRAF has been one

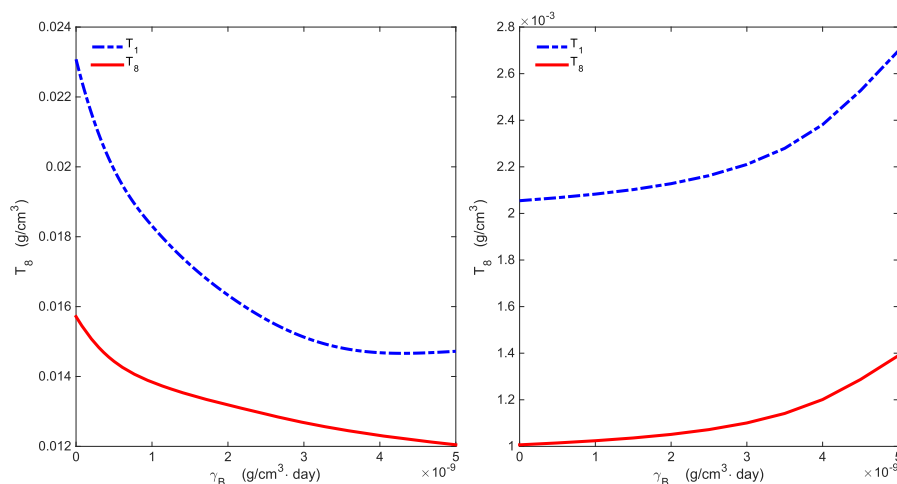


Fig. 5 Average densities of T_1 and T_8 . **a** Average densities of T_1 and T_8 decrease as γ_B increases for fixed $\gamma_A = 1.26 \times 10^{-9} \text{ g/cm}^3 \cdot \text{day}$; **b**. Average densities of T_1 and T_8 increase as γ_B increases for fixed $\gamma_A = 0.14 \times 10^{-9} \text{ g/cm}^3 \cdot \text{day}$. Here, γ_B varies between $0 - 5 \times 10^{-9} \text{ g/cm}^3 \cdot \text{day}$ and all other parameter values are the same as in Tables 2 and 3

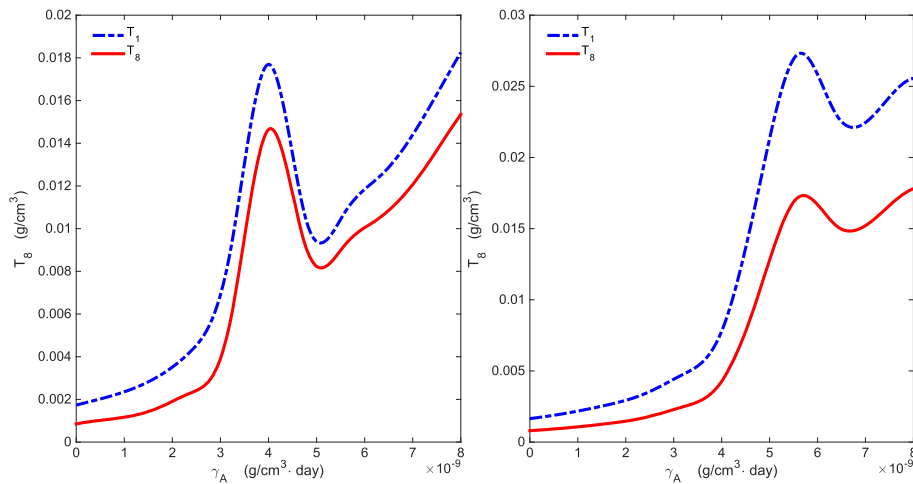


Fig. 6 Average densities of T_1 and T_8 . **a** There is a γ_A -interval where average densities of T_1 and T_8 are decreasing as γ_A increases for fixed $\gamma_B = 3 \times 10^{-9} \text{ g/cm}^3 \cdot \text{day}$. **b** The γ_A -interval where average T_1 and T_8 are decreasing may shrink as γ_B is taken to be smaller, e.g. $\gamma_B = 0.1 \times 10^{-9} \text{ g/cm}^3 \cdot \text{day}$. Here, γ_A varies between $n.4 \times 10^{-9} \text{ g/cm}^3 \cdot \text{day}$ and all other parameter values are the same as in Tables 2 and 3

of the primary targets in melanoma therapy. Treatment with BRAF inhibitors (such as vemurafenib or dabrafenib) encounters MAPK-driven resistance, but combining it with MEK inhibitor (e.g. trametinib) significantly reduces this resistance as well as toxicity. While the response to the combined BRAF/MEK inhibitor is significant, it is short lived. On the other hand, PD-1 antibody (nivolumab) has lower response rate but a far greater durability. It was therefore suggested that BRAF/MEK inhibitor should positively correlate with anti-PD-1.

In the present paper we developed a mathematical model to test this hypothesis, *in silico*, by computing the efficacy of the combined therapy. The model is represented by a system of partial differential equations within the tumor tissue. The model includes immune cells (Th1 and CD8⁺ T cells, Tregs, MDSCs and dendritic cells), cytokines (IL-12, IL-2, IL-6, IL-10 and TGF- β), and PD-1, PD-L1 and the complex PD-1-PD-L1. We simulated the model with combination of drugs, BRAF/MEK inhibitor at the ‘level’ γ_B and PD-1 antibody at the ‘level’ γ_A , and computed the tumor radius $R_{60} = R_{60}(\gamma_A, \gamma_B)$ at day 60, and the efficacy $E(\gamma_B, \gamma_A) = \frac{R_{60}(0,0) - R_{60}(\gamma_B, \gamma_A)}{R_{60}(0,0)}$; the efficacy is an expression that quantifies the reduction in tumor size compared to the control case (no drugs).

The efficacy map in Fig. 4 shows that for low levels of γ_B and γ_A , the two drugs are positively correlated, in the sense that tumor volume decreases as each of the drugs is increased. However, in the ‘northeast’ corner of Fig. 4 we see that for higher levels of γ_B and γ_A there are zones where the drugs are antagonistic in the sense that when γ_B and γ_A in these zones are increased, the efficacy actually decreases. The antagonism between the combined drugs can be explained by the pathway shown in Fig. 7. An increase in the number of effector T cells (Th1 and CD8⁺) results in decrease in cancer cells and necrotic cancer cells, hence in decreased signals to activate dendritic cells. This results in a decrease in IL-12 production by dendritic cells, and hence in a decrease in effector T cells.

The parameter $\lambda_{I_{12}B}$ may be viewed as the immune system response to BRAF/MEK inhibitor. When this parameter is increased, the antagonism in the combined therapy is reduced, but it does not completely disappear (not shown here).

The mathematical model presented in this paper has several limitations:

- (i) In order to focus on the combined therapy of a BRAF/MEK inhibitor and an anti-PD-1 drug, we did

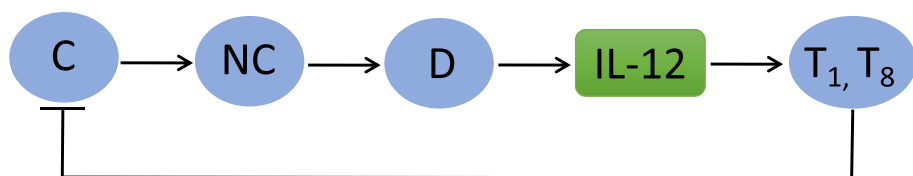


Fig. 7 Antagonistic pathway between C and (T_1, T_8)

Table 2 Summary of parameter values

| Notation | Description | Value used | References |
|-------------------------|---|---|------------|
| δ_D | Diffusion coefficient of DCs | $8.64 \times 10^{-7} \text{ cm}^2 \text{ day}^{-1}$ | [65] |
| δ_T | Diffusion coefficient of T cells | $8.64 \times 10^{-7} \text{ cm}^2 \text{ day}^{-1}$ | [65] |
| δ_M | Diffusion coefficient of MDSCs | $8.64 \times 10^{-7} \text{ cm}^2 \text{ day}^{-1}$ | [65] |
| δ_C | Diffusion coefficient of tumor cells | $8.64 \times 10^{-7} \text{ cm}^2 \text{ day}^{-1}$ | [65] |
| $\delta_{I_{12}}$ | Diffusion coefficient of IL-12 | $6.05 \times 10^{-2} \text{ cm}^2 \text{ day}^{-1}$ | Estimated |
| δ_{I_2} | Diffusion coefficient of IL-2 | $9.58 \times 10^{-2} \text{ cm}^2 \text{ day}^{-1}$ | Estimated |
| δ_{T_β} | Diffusion coefficient of TGF- β | $8.52 \times 10^{-2} \text{ cm}^2 \text{ day}^{-1}$ | Estimated |
| δ_{I_6} | Diffusion coefficient of IL-6 | $9.03 \times 10^{-2} \text{ cm}^2 \text{ day}^{-1}$ | Estimated |
| $\delta_{I_{10}}$ | Diffusion coefficient of IL-10 | $9.11 \times 10^{-2} \text{ cm}^2 \text{ day}^{-1}$ | Estimated |
| δ_A | Diffusion coefficient of anti-PD-1 | $7.85 \times 10^{-2} \text{ cm}^2 \text{ day}^{-1}$ | Estimated |
| δ_B | Diffusion coefficient of BRAF/MEKi | $3.16 \times 10^{-1} \text{ cm}^2 \text{ day}^{-1}$ | Estimated |
| σ_0 | Flux rate of T_1 and T_8 cells at the boundary | 1 cm^{-1} | [65] |
| χ | Chemoattraction coefficient of IL-6 | $10 \text{ cm}^5/\text{g} \cdot \text{day}$ | [90, 91] |
| λ_{DC} | Activation rate of DCs by tumor cells | $4 \text{ g/cm}^3 \cdot \text{day}$ | [65] |
| $\lambda_{T_1 I_{12}}$ | Activation rate of $CD4^+$ T cells by IL-12 | 18.64 day^{-1} | Estimated |
| $\lambda_{T_1 I_2}$ | Activation rate of $CD4^+$ T cells by IL-2 | 0.25 day^{-1} | [65] |
| $\lambda_{T_8 I_{12}}$ | Activation rate of $CD8^+$ T cells by IL-12 | 16.6 day^{-1} | Estimated |
| $\lambda_{T_8 I_2}$ | Activation rate of $CD8^+$ T cells by IL-2 | 0.25 day^{-1} | [65] |
| $\lambda_{T_r T_\beta}$ | Activation rate of Tregs by TGF- β | 0.415 day^{-1} | Estimated |
| $\lambda_{T_r Q}$ | Activation rate of Tregs by PD-1-PD-L1 | 0.083 day^{-1} | Estimated |
| λ_M | Activation rate of MDSCs | 1.05 day^{-1} | [40] |
| λ_C | Growth rate of cancer cells | 0.616 day^{-1} | Estimated |
| λ_0 | Growth rate of cancer cells uninhibited (by immune cells) | 0.069 day^{-1} | Estimated |
| $\lambda_{I_{12} D}$ | Production rate of IL-12 by DCs | $2.76 \times 10^{-6} \text{ day}^{-1}$ | Estimated |
| $\lambda_{I_{12} B}$ | Promotion of IL-12 production by BRAF/MEKi | 1 | Estimated |
| $\lambda_{I_2 T_1}$ | Production rate of IL-2 by $CD4^+$ T cells | $2.82 \times 10^{-8} \text{ day}^{-1}$ | Estimated |
| $\lambda_{T_\beta C}$ | Production rate of TGF- β by cancer cells | $2.18 \times 10^{-10} \text{ day}^{-1}$ | Estimated |
| $\lambda_{T_\beta T_r}$ | Production rate of TGF- β by Tregs | $5.57 \times 10^{-9} \text{ day}^{-1}$ | [75] |
| $\lambda_{T_\beta M}$ | Production rate of TGF- β by MDSCs | $2.18 \times 10^{-10} \text{ day}^{-1}$ | Estimated |
| $\lambda_{I_6 C}$ | Production rate of IL-6 by cancer cells | $3.54 \times 10^{-10} \text{ day}^{-1}$ | Estimated |
| $\lambda_{I_{10} C}$ | Production rate of IL-10 by cancer cells | $9.10 \times 10^{-10} \text{ day}^{-1}$ | Estimated |
| $\lambda_{I_{10} M}$ | Production rate of IL-10 by MDSCs | $1.82 \times 10^{-9} \text{ day}^{-1}$ | Estimated |
| η_1 | Killing rate of tumor cells by $CD4^+$ T cells | $11.5 \text{ day}^{-1} \cdot \text{cm}^3/\text{g}$ | Estimated |
| η_8 | Killing rate of tumor cells by $CD8^+$ T cells | $46 \text{ day}^{-1} \cdot \text{cm}^3/\text{g}$ | Estimated |
| μ_{PA} | Blocking rate of PD-1 by anti-PD-1 | $6.04 \times 10^6 \text{ cm}^3/\text{g} \cdot \text{day}$ | Estimated |
| μ_{BC} | Absorbtion rate of BRAF/MEKi by cancer cells | $6.17 \times 10^{-10} \text{ day}^{-1}$ | Estimated |
| ρ_P | Expression of PD-1 in T cells | 2.49×10^{-7} | Estimated |
| ρ_L | Expression of PD-L1 in T cells | 5.22×10^{-7} | Estimated |
| ε_C | Expression of PD-L1 in tumor cells | 0.01 | [84] |
| ε_M | Expression of PD-L1 in MDSCs | 0.005 | Estimated |
| d_D | Death rate of DCs | 0.1 day^{-1} | [65] |
| d_{T_1} | Death rate of $CD4^+$ T cells | 0.197 day^{-1} | [65] |
| d_{T_8} | Death rate of $CD8^+$ T cells | 0.18 day^{-1} | [65] |
| d_{T_r} | Death rate of Tregs | 0.2 day^{-1} | [75] |

Table 2 Summary of parameter values (*Continued*)

| | | | |
|---------------|---|--------------------------------------|-----------|
| d_M | Death rate of MDSCs | 0.03 day ⁻¹ | [40] |
| d_C | Death rate of tumor cells | 0.17 day ⁻¹ | [65] |
| $d_{I_{12}}$ | Degradation rate of IL-12 | 1.38 day ⁻¹ | [65] |
| d_{I_2} | Degradation rate of IL-2 | 2.376 day ⁻¹ | [65] |
| d_{T_β} | Degradation rate of TGF- β | 499.066 day ⁻¹ | Estimated |
| d_{I_6} | Degradation rate of IL-6 | 4.16 day ⁻¹ | Estimated |
| $d_{I_{10}}$ | Degradation rate of IL-10 | 8.32 day ⁻¹ | Estimated |
| d_A | Degradation rate of anti-PD-1 | 0.046 day ⁻¹ | [87] |
| d_B | Degradation rate of BRAF/MEKi | 1.66day ⁻¹ | Estimated |
| D_0 | Density of inactive DCs | 2×10^{-5} g/cm ³ | [65] |
| T_{10} | Density of naive CD4 ⁺ T cells in tumor | 4×10^{-4} g/cm ³ | Estimated |
| T_{80} | Density of naive CD8 ⁺ T cells in tumor | 2×10^{-4} g/cm ³ | Estimated |
| C_M | Carrying capacity of cancer cells | 0.8 g/cm ³ | [65] |
| \hat{T}_1 | Density of CD4 ⁺ T cells from lymph node | 4×10^{-3} g/cm ³ | Estimated |
| \hat{T}_8 | Density of CD8 ⁺ T cells from lymph node | 2×10^{-3} g/cm ³ | Estimated |

not include in the model the effect of angiogenesis, thus assuming that the tumor is avascular. We tacitly assumed that the effect of this omission is not significant in comparing the results of therapy to no therapy.

- (ii) We assumed that the densities of immature, or naive, immune cells remain constant throughout the progression of the cancer and that density of debris of dead cells is constant.
- (iii) We assumed that the process of necrosis is fast, and that the density of cancer cells undergoing necrosis is at steady state.
- (iv) In estimating parameters we made a steady state assumption in some of the differential equations.

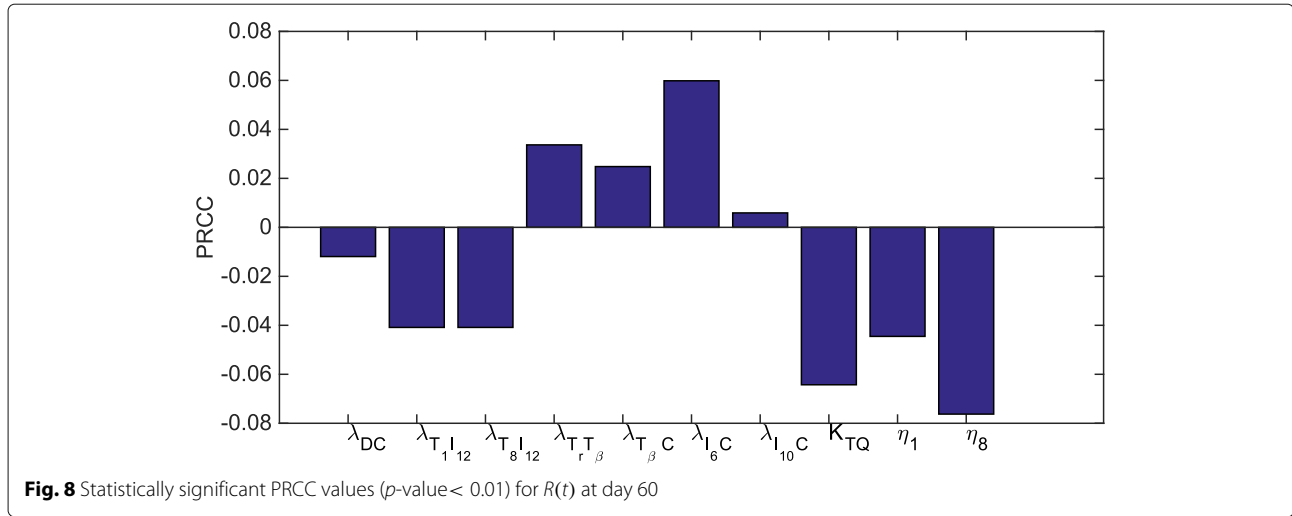
- (v) We did not make any direct connection between drugs administered to the patient, and their 'effective strengths' γ_B and γ_A , as they appear in the differential equations, since these data are not available.

A general study of synergistic and antagonistic networks in drug combinations appeared in [47]. Clinical records on combination therapy show that the number of drugs that are synergistic far exceeds the number of drugs that are antagonistic [48].

In our model, the combination (γ_B, γ_A) is antagonistic when the drugs are administered in high doses, but not in low doses. For this reason it will be important to identify more carefully the zones of antagonism, by animal exper-

Table 3 Summary of parameter values

| Notation | Description | Value used | References |
|---------------|--|--|------------|
| K_{T_1} | Half-saturation of CD4 ⁺ T cells | 2×10^{-3} g/cm ³ | Estimated |
| K_{T_8} | Half-saturation of CD8 ⁺ T cells | 1×10^{-3} g/cm ³ | Estimated |
| K_{T_r} | Half-saturation of Tregs | 5×10^{-4} g/cm ³ | [65] |
| K_C | Half-saturation of tumor cells | 0.4 g/cm ³ | [65] |
| $K_{I_{12}}$ | Half-saturation of IL-12 | 8×10^{-10} g/cm ³ | Estimated |
| K_{I_2} | Half-saturation of IL-2 | 2.37×10^{-11} g/cm ³ | [65] |
| K_{T_β} | Half-saturation of TGF- β | 2.68×10^{-13} g/cm ³ | Estimated |
| K_{I_6} | Half-saturation of IL-6 | 3.4×10^{-11} g/cm ³ | Estimated |
| $K_{I_{10}}$ | Half-saturation of IL-10 | 8.75×10^{-11} g/cm ³ | Estimated |
| K'_Q | Half-saturation of PD-1-PD-L1 | 3.54×10^{-18} g ² /cm ⁶ | Estimated |
| K_B | Half-saturation of BRAF/MEKi | 6.69×10^{-10} g/cm ³ | Estimated |
| K'_{TQ} | Inhibition of function of T cells by PD-1-PD-L1 | 1.77×10^{-18} g ² /cm ⁶ | Estimated |
| K_{CB} | Inhibition of proliferation of cancer cells by BRAF/MEKi | 3.06×10^{-9} g/cm ³ | Estimated |



iments or by early clinical trials, in order to avoid those zones in more advanced clinical trials.

Appendix

Parameter estimation

Half-saturation

In an expression of the form $Y \frac{X}{K_X + X}$ where Y is activated by X , the half-saturation parameter K_X is taken to be the approximate steady state concentration of species X .

Diffusion coefficients

By [49], we have the following relation for estimating the diffusion coefficients of a protein p :

$$\delta_p = \frac{M_V^{1/3}}{M_p^{1/3}} \delta_V,$$

where M_V and δ_V are respectively the molecular weight and diffusion coefficient of VEGF, M_p is the molecular weight of p , and $M_V = 24\text{kDa}$ [50] and $\delta_V = 8.64 \times 10^{-2} \text{ cm}^2 \text{ day}^{-1}$ [51]. Since, $M_{I_2} = 17.6\text{kDa}$ [52], $M_{I_{12}} = 70\text{kDa}$ [53], $M_{T_\beta} = 25\text{kDa}$ [54], $M_{I_6} = 21\text{kDa}$ [55, 56], $M_{I_{10}} = 20.5\text{kDa}$ [57], $M_A = 32\text{kDa}$ [58] and $M_B = 489.93\text{kDa}$ [59], we get $\delta_{I_2} = 9.58 \times 10^{-2} \text{ cm}^2 \text{ day}^{-1}$, $\delta_{I_{12}} = 6.05 \times 10^{-2} \text{ cm}^2 \text{ day}^{-1}$, $\delta_{T_\beta} = 8.52 \times 10^{-2} \text{ cm}^2 \text{ day}^{-1}$, $\delta_{I_6} = 9.03 \times 10^{-2} \text{ cm}^2 \text{ day}^{-1}$, $\delta_{I_{10}} = 9.11 \times 10^{-2} \text{ cm}^2 \text{ day}^{-1}$, $\delta_A = 7.85 \times 10^{-2} \text{ cm}^2 \text{ day}^{-1}$ and $\delta_B = 3.16 \times 10^{-1} \text{ cm}^2 \text{ day}^{-1}$.

Equation (2)

The number of DCs in various organs (heart, kidney, pancreas and liver) in mouse varies from $1.1 \times 10^6 \text{ cells/cm}^3$ to $6.6 \times 10^6 \text{ cells/cm}^3$ [60]. In the dermal tissue, the number of DCs is larger ($600\text{-}1500 \text{ cells/mm}^2$) [61, 62], but we do not specify where the melanoma cancer is located; it may be at its initial dermal tissue or in another organ where it metastasized.

Mature DCs are approximately 10 to 15 μm in diameter [63]. Accordingly, we estimate the steady state of DCs to be $K_D = 4 \times 10^{-4} \text{ g/cm}^3$. We assume that there are always immature dendritic cells, some coming from the blood as tumor infiltrating dendritic cells (TID) [20, 21, 64]. We also assume that the density of immature DCs to be smaller than the density of active DCs, and take $D_0 = \frac{1}{20} K_D = 2 \times 10^{-5} \text{ g/cm}^3$. From the steady state of Eq. (2), we get $\lambda_{DC} = 2d_D D/D_0 = 4/\text{day}$, since $d_D = 0.1/\text{day}$ [65]. We take $K_C = 0.4 \text{ g/cm}^3$.

Equation (3)

The number of lymphocytes is approximately twice the number of DCs [60]. T cells are approximately 14 to 20 μm in diameter. Assuming that the number of Th1 cells is 1/4 the number of lymphocytes, we estimate steady state density of Th1 cells to be $K_{T_1} = 2 \times 10^{-3} \text{ g/cm}^3$. We assume that the density of naive $CD4^+$ T cells to be less than the density of Th1, and take $T_{10} = \frac{1}{5} K_T = 4 \times 10^{-4} \text{ g/cm}^3$. As in [65], we choose $K_{T T_r}$ to be half-saturation of T_r , that is, $K_{T T_r} = 5 \times 10^{-4} \text{ g/cm}^3$, and as in [66], we choose $K_{T I_{10}}$ to be half-saturation of I_{10} , namely, $K_{T I_{10}} = 2 \times 10^{-7} \text{ g/cm}^3$. We assume that in steady state, $Q/K_{TQ} = 2$ (the value of K_{TQ} is derived in the estimates of Eqs. (13)-(15)). From the steady state of Eq. (3), we get

$$\left(\lambda_{T_1 I_{12}} T_{10} \cdot \frac{1}{2} \cdot \frac{1}{2} \cdot \frac{1}{2} + \lambda_{T_1 I_2} T_1 \cdot \frac{1}{2} \right) \cdot \frac{1}{3} - d_{T_1} T_1 = 0,$$

where $\lambda_{T_1 I_2} = 0.25/\text{day}$ [65], $d_{T_1} = 0.197/\text{day}$ [65], $T_{10} = 4 \times 10^{-4} \text{ g/cm}^3$ and $T_1 = K_{T_1} = 2 \times 10^{-3} \text{ g/cm}^3$. Hence $\lambda_{T_1 I_{12}} = 18.64/\text{day}$.

Equation (4)

The $CD4/CD8$ ratio in the blood is 2:1. We assume a similar ratio in tissue, and take $T_{80} = \frac{1}{2} T_{10} = 2 \times 10^{-4} \text{ g/cm}^3$. We also take steady state of T_8 to be the half of steady state

of T_1 , i.e., $K_{T_8} = \frac{1}{2}K_{T_1} = 1 \times 10^{-3} \text{ g/cm}^3$. From the steady state of Eq. (4), we have

$$\left(\lambda_{T_8 I_{12}} T_{80} \cdot \frac{1}{2} \cdot \frac{1}{2} \cdot \frac{1}{2} + \lambda_{T_1 I_2} T_8 \cdot \frac{1}{2} \right) \cdot \frac{1}{3} - d_{T_8} T_8 = 0$$

where $\lambda_{T_8 I_2} = 0.25/\text{day}$ [65], $d_{T_8} = 0.18/\text{day}$ [65], $T_{80} = 2 \times 10^{-4} \text{ g/cm}^3$, $T_8 = K_{T_8} = 1 \times 10^{-3} \text{ g/cm}^3$. Hence $\lambda_{T_8 I_{12}} = 16.6/\text{day}$.

Equation (5)

We assume that TGF- β activates Tregs more than PD-1-PD-L1 does, and take $\lambda_{T_r T_\beta} = 5\lambda_{T_r Q}$. From the steady state of Eq. (5), we get, $(\lambda_{T_r T_\beta} \cdot \frac{1}{2} + \lambda_{T_r Q} \cdot \frac{1}{2}) T_{10} - d_{T_r} T_r = 0$, where $T_{10} = 1 \times 10^{-3} \text{ g/cm}^3$, $T_r = K_{T_r} = 5 \times 10^{-4} \text{ g/cm}^3$ [65], and $d_{T_r} = 0.2/\text{day}$ [65]. Hence $\lambda_{T_r Q} = 0.083/\text{day}$ and $\lambda_{T_r T_\beta} = 0.415/\text{day}$.

Equation (6)

The density of tumor-associated macrophages in melanoma can be up to 30% of the tumor tissue density [67]; we take MDSC density to be 20% of the tumor tissue density, so that $M = 0.2 \text{ g/cm}^3$ in steady state. From the steady state of Eq. (6), we get, $\frac{1}{2}\lambda_M(M_0 - M) = d_M M$, where $d_M = 0.015/\text{day}$ [40], $\lambda_M = 20/19 = 1.05$ [40], and $M = K_M = 0.2 \text{ g/cm}^3$. Hence, $M_0 = 0.21 \text{ g/cm}^3$.

Equation (7)

We take $d_C = 0.17 \text{ day}^{-1}$ and $C_M = 0.8 \text{ g/cm}^3$ [65]. In the control case (no anti-tumor drugs), the tumor grows according to

$$\frac{dC}{dt} = \lambda_C C \left(1 - \frac{C}{C_M} \right) - (\eta_1 T_1 + \eta_8 T_8) C - d_C C. \quad (23)$$

Mouse experiments show that tumor volume doubles within 5 -15 days [44, 68–70]. Assuming a linear growth

$$\frac{dC}{dt} = \lambda_0 C, \quad \text{where } \lambda_0 > 0,$$

during the volume doubling time in the control case, we conclude from Eq. (23) that

$$\lambda_C C \left(1 - \frac{C}{C_M} \right) - (\eta_1 T_1 + \eta_8 T_8) C - d_C C = \lambda_0 C. \quad (24)$$

where $\lambda_0 \in \left(\frac{\ln 2}{15}, \frac{\ln 2}{5} \right)$. We assume that without immune responses and BRAF/MEK inhibitor,

$$\frac{dC}{dt} = 2\lambda_0 C,$$

so that

$$\lambda_C C \left(1 - \frac{C}{C_M} \right) - d_C C = 2\lambda_0 C. \quad (25)$$

We further assume that with immune response and BRAF/MEK inhibitor, the density of cancer cell still grows,

$$\frac{dC}{dt} = \frac{1}{5}\lambda_0 C,$$

so that

$$\lambda_C C \left(1 - \frac{C}{C_M} \right) \cdot \frac{1}{1+B/K_{CB}} - (\eta_1 T_1 + \eta_8 T_8) C - d_C C = \frac{1}{5}\lambda_0 C. \quad (26)$$

We take $\lambda_0 = 0.069/\text{day}$, and assume that in steady state, C is approximately 0.4 g/cm^3 , so that from Eq. (25) we get $\frac{1}{2}\lambda_C - d_C = 2\lambda_0$, or $\lambda_C = 2(2\lambda_0 + d_C) = 0.616/\text{day}$. By comparing Eq. (24) to Eq. (25), we see that $\eta_1 T_1 + \eta_8 T_8 = \lambda_0$. Noting that T_8 cells kill cancer cells more effectively than T_1 cells, we take $\eta_8 = 4\eta_1$, so that (with $T_1 = K_{T_1} = 2 \times 10^{-3} \text{ g/cm}^3$ and $T_8 = K_{T_8} = 1 \times 10^{-3} \text{ g/cm}^3$) $\eta_1 = \frac{\lambda_0}{T_1 + 4T_8} = 11.5 \text{ cm}^3/\text{g} \cdot \text{day}$ and $\eta_8 = 46 \text{ cm}^3/\text{g} \cdot \text{day}$. From Eq. (26), we have $\frac{1}{2}\lambda_C \cdot \frac{1}{1+B/K_{CB}} - (\eta_1 T_1 + \eta_8 T_8) - d_C = \frac{1}{5}\lambda_0$. Since $\lambda_C = 2(2\lambda_0 + d_C)$ and $\eta_1 T_1 + \eta_8 T_8 = \lambda_0$, we get $(2\lambda_0 + d_C) \cdot \frac{1}{1+B/K_{CB}} - \lambda_0 - d_C = \frac{1}{5}\lambda_0$, so that (with $B = K_B = 6.69 \times 10^{-10} \text{ g/cm}^3$) $K_{CB} = B \frac{5d_C + 6\lambda_0}{4\lambda_0} = 3.06 \times 10^{-9} \text{ g/cm}^3$.

Equation (8)

The serum level of IL-12 in melanoma patients varies from $7.5 \times 10^{-11} - 9.6 \times 10^{-11} \text{ g/cm}^3$ [71, 72]. We assume that the IL-12 level in tissue is higher, and take $I_{12} = K_{I_{12}} = 8 \times 10^{-10} \text{ g/cm}^3$. In the control case (no drugs), from the steady state of Eq. (8), we get $\lambda_{I_{12} D} D - d_{I_{12}} I_{12} = 0$, where $d_{I_{12}} = 1.38/\text{day}$ [65] and $D = K_D = 4 \times 10^{-4} \text{ g/cm}^3$. Hence, $\lambda_{I_{12} D} = 2.76 \times 10^{-6}/\text{day}$. In the simulations we take $\lambda_{I_{12} B} = 1$, but simulations do not change qualitatively with smaller or larger values of $\lambda_{I_{12} B}$.

Equation (9)

From the steady state of Eq. (9), we get $\lambda_{I_2 T_1} T_1 - d_{I_2} I_2 = 0$, where $d_{I_2} = 2.376/\text{day}$ [65] and $I_2 = K_{I_2} = 2.37 \times 10^{-11} \text{ g/cm}^3$ [65], and $T_1 = K_{T_1} = 2 \times 10^{-3} \text{ g/cm}^3$. Hence, $\lambda_{I_2 T_1} = 2.82 \times 10^{-8}/\text{day}$.

Equation (10)

The half-life of TGF- β is about 2 min [73], that is, $t_{1/2} = 0.0014 \text{ day}$, so that $d_{T_\beta} = \ln 2/t_{1/2} = 499.07 \text{ day}^{-1}$. The concentration of serum TGF- β in melanoma is $2.68 \times 10^{-14} \text{ g/cm}^3$ [74]. We assume that the concentration of TGF- β in tissue is higher than in serum, and take $T_\beta = 2.68 \times 10^{-13} \text{ g/cm}^3$. By [75], $\lambda_{T_\beta T_r} = 5.57 \times 10^{-9}/\text{day}$. According to [27, 42], melanoma cells secrete more TGF- β than MDSC, and we assume that $\lambda_{T_\beta C} C = 2\lambda_{T_\beta M} M$. Hence, from the steady state of Eq. (10) we have, $\lambda_{T_\beta C} C + \lambda_{T_\beta M} M + \lambda_{T_\beta T_r} T_r = d_{T_\beta} T_\beta$, or $3\lambda_{T_\beta M} M + \lambda_{T_\beta T_r} T_r = d_{T_\beta} T_\beta$. Thus $\lambda_{T_\beta M} = (d_{T_\beta} T_\beta - \lambda_{T_\beta T_r} T_r)/(3M) = 2.18 \times 10^{-10}/\text{day}$, and $\lambda_{T_\beta C} = 2\lambda_{T_\beta M} M/C = 2.18 \times 10^{-10}/\text{day}$.

Equation (11)

The half-life of IL-6 is less than 6 hours [76], and we take it to be 4 hours, that is, $t_{1/2} = 0.17$ day, so that $d_{I_6} = \ln 2/t_{1/2} = 4.16 \text{ day}^{-1}$. The concentration of serum IL-6 in melanoma is $3.4 \times 10^{-12} \text{ g/cm}^3$ [77]. We assume that the concentration of IL-6 in tissue is higher than in serum, and take $I_6 = 3.4 \times 10^{-11} \text{ g/cm}^3$. From the steady state of Eq. (11), we get $\lambda_{I_6 C} = d_{I_6} I_6 / C = 3.54 \times 10^{-10} / \text{day}$.

Equation (12)

The half-life of IL-10 ranges from 1.1 to 2.6 hours [78]; we take it to be 2 hours, that is, $t_{1/2} = 0.08$ day, so that $d_{I_{10}} = 8.32 \text{ day}^{-1}$. The concentration of serum IL-10 in melanoma is $8.75 \times 10^{-12} \text{ g/cm}^3$ [79]. We assume that the concentration of IL-10 in tissue is higher than in serum, and take $I_{10} = 8.75 \times 10^{-11} \text{ g/cm}^3$. In melanoma, the tissue concentrations of IL-10 secreted by tumor cells and by macrophages are similar [80], and, accordingly, we assume that $\lambda_{I_{10} C} = \lambda_{I_{10} M}$ in steady state. Hence, from the steady state of Eq. (12) we get, $2\lambda_{I_{10} C} C - d_{I_{10}} I_{10} = 0$, so that $\lambda_{I_{10} C} = d_{I_{10}} I_{10} / 2C = 9.10 \times 10^{-10} / \text{day}$, and $\lambda_{I_{10} M} = \lambda_{I_{10} C} C / M = 1.82 \times 10^{-9} / \text{day}$.

Equations (13)-(15)

In order to estimate the parameters K_{TQ} (in Eqs. (3) and (4)) and K_Q (in Eq. (5)), we need to determine the steady state concentrations of P and L in the control case (no drugs). To do that, we begin by estimating ρ_P and ρ_L .

By [81], the mass of one PD-1 is $m_P = 8.3 \times 10^{-8} \text{ pg} = 8.3 \times 10^{-20} \text{ g}$, and by [1] the mass of one PD-L1 is $m_L = 5.8 \times 10^{-8} \text{ pg} = 5.8 \times 10^{-20} \text{ g}$. We assume that the mass of one T cell is $m_T = 10^{-9} \text{ g}$. By [82], there are 3000 PD-1 proteins and 9000 PD-L1 proteins on one T cell (T_1 or T_8). Since $\rho_P T$ is the density of PD-1 (without anti-PD-1 drug), we get $\rho_P = 3000 \times \frac{m_P}{m_T} = \frac{3000 \times (8.3 \times 10^{-20})}{10^{-9}} = 2.49 \times 10^{-7}$, and $\rho_L = 9000 \times \frac{m_L}{m_T} = \frac{9000 \times (5.8 \times 10^{-20})}{10^{-9}} = 5.22 \times 10^{-7}$.

In order to estimate steady state concentration of P , we assume that the average densities of T_1 , T_8 and T_r are approximately 2×10^{-3} , 1×10^{-3} and $5 \times 10^{-4} \text{ g/cm}^3$, respectively. PD-1 is expressed by Tregs at higher or lower level than in T_1 and T_8 cells depending on the type of the cancer [83]; we assume that $\varepsilon_T = 0.8$. Hence, in steady state,

$$\begin{aligned} P &= \rho_P(T_1 + T_8 + \varepsilon_T T_r) \\ &= (2.49 \times 10^{-7}) \times [2 \times 10^{-3} + 1 \times 10^{-3} + 0.8 \times (5 \times 10^{-4})] \\ &= 8.46 \times 10^{-10} \text{ g/cm}^3. \end{aligned}$$

The parameter ε_C in Eq. (14) depends on the type of cancer. We take $\varepsilon_C = 0.01$ [84]. MDSCs express PD-L1 at lower level than tumor cells [85], and accordingly, we

assume that $\varepsilon_M M = \frac{1}{4} \varepsilon_C C$, so that $\varepsilon_M = \varepsilon_C C / 4M = \varepsilon_C / 2 = 0.005$. Then, by Eq. (14), we get

$$\begin{aligned} L &= \rho_L(T_1 + T_8 + \varepsilon_M M + \varepsilon_C C) \\ &= (5.22 \times 10^{-7}) \times [3 \times 10^{-3} + 0.005 \times 0.2 + 0.01 \times 0.4] \\ &= 4.176 \times 10^{-9} \text{ g/cm}^3. \end{aligned}$$

In steady state with $P = \bar{P}$, $L = \bar{L}$ and $Q = \bar{Q}$, we have, by Eq. (15), $\bar{Q} = \sigma \bar{P} \bar{L}$. We take $K_{TQ} = \frac{1}{2} \bar{Q} = \frac{1}{2} \sigma \bar{P} \bar{L}$. Hence, $Q/K_{TQ} = PL / (\frac{1}{2} \bar{P} \bar{L})$ and

$$\frac{1}{1 + Q/K_{TQ}} = \frac{1}{1 + PL / (\frac{1}{2} \bar{P} \bar{L})} = \frac{1}{1 + PL/K'_{TQ}},$$

where $K'_{TQ} := \frac{1}{2} \bar{P} \bar{L} = \frac{1}{2} \times (8.46 \times 10^{-10}) \times (4.176 \times 10^{-9}) = 1.77 \times 10^{-18} \text{ g}^2 / \text{cm}^6$. Similarly, $K_Q = \bar{Q} = \sigma \bar{P} \bar{L}$, so that in Eq. (5),

$$\frac{Q}{K_Q + Q} = \frac{1}{1 + K_Q/Q} = \frac{1}{1 + \bar{P} \bar{L} / PL} = \frac{1}{1 + K'_Q / PL},$$

where $K'_Q := \bar{P} \bar{L} = 3.54 \times 10^{-18} \text{ g}^2 / \text{cm}^6$.

Equations (16)-(17)

In mice experiments [44, 86] different amounts of drugs were injected, and the amount of BRAF/MEK inhibitor was larger than the amount of anti-PD-1. It is difficult to compare the amounts injected into mice with the actual levels of the drugs which appear in Eqs. (16) and (17), since there is no information available on the PK/PD of the drugs. For the choice of $\gamma_A = 0.3 \times 10^{-9} \text{ g/cm}^3 \cdot \text{day}$ and $\gamma_B = 0.5 \times 10^{-9} \text{ g/cm}^3 \cdot \text{day}$, we found that the simulations are in qualitative agreement with experiments reported in [44]. We shall accordingly take γ_A in the range of $n.4 \times 10^{-9} \text{ g/cm}^3 \cdot \text{day}$ and γ_B in the range of $0 - 5 \times 10^{-9} \text{ g/cm}^3 \cdot \text{day}$.

By [87], the half-life of anti-PD-1 is 15 days, so that $d_A = \frac{\ln 2}{15} = 0.046 \text{ day}^{-1}$. We assume that 10% of A is used in blocking PD-1, while the remaining 90% degrades naturally. Hence, $\mu_{PA} PA / 10\% = d_A A / 90\%$, so that

$$\mu_{PA} = \frac{d_A}{9P} = \frac{0.046}{9 \times (8.46 \times 10^{-10})} = 6.04 \times 10^6 \text{ cm}^3 / \text{g} \cdot \text{day}.$$

The half-life of BRAF inhibitor (dabrafenib) is 8 hours [88], and the half-life of MEK inhibitor (trametinib) is 33 h [89]. In the combination of BRAF/MEKi, the proportion of MEKi is smaller than BRAFi [44], and accordingly we take the half-life of BRAF/MEKi to be 10 h, so that $d_B = \frac{\ln 2}{10/24} = 1.66 \text{ day}^{-1}$. We assume that 10% of B is absorbed by cancer cells, while the remaining 90% degrades naturally, so that $\mu_{BC} C \frac{B}{K_B + B} / 10\% = d_B B / 90\%$. From Eq. (17), we get $B \geq \gamma_B / d_B$, and we assume that

$$B \sim \frac{10}{9} \cdot \frac{\gamma_B}{d_B},$$

where $d_B = 1.66 / \text{day}$. We take γ_B to be order of magnitude $10^{-9} \text{ g/cm}^3 \cdot \text{day}$ in the simulations. Hence, $B = K_B =$

6.69×10^{-10} g/cm³ in steady state, and $\mu_{BC} = 2d_B B/9C = 6.17 \times 10^{-10}$ /day.

Eqs. (20): We assume that \hat{T}_1 is larger than K_{T_1} and take $\hat{T}_1 = 4 \times 10^{-3}$ g/cm³. Similarly, we also assume that \hat{T}_8 is larger than K_{T_8} and take $\hat{T}_8 = 2 \times 10^{-3}$ g/cm³.

Computational method

We employ moving mesh method [45] to numerically solve the free boundary problem for the tumor proliferation model. To illustrate this method, we take Eq. (2) as example and rewrite it as the following form:

$$\frac{\partial D(r, t)}{\partial t} = \delta_D \Delta D(r, t) - \text{div}(\mathbf{u}D) + F, \quad (27)$$

where F represents the term in the right hand side of Eq. (2). Let r_i^k and D_i^k denote numerical approximations of i -th grid point and $D(r_i^k, n\tau)$, respectively, where τ is the size of time-step. The discretization of Eq. (27) is derived by the fully implicit finite difference scheme:

$$\frac{D_i^{k+1} - D_i^k}{\tau} = \delta_D \left(D_{rr} + \frac{2}{r_i^k} D_r \right) - \left(\frac{2}{r_i^{k+1}} u_i^{k+1} + u_r \right) D_i^{k+1} - u_i^{k+1} D_r + F_i^{k+1}, \quad (28)$$

where $D_r = \frac{h_{-1}^2 D_{i+1}^{k+1} - h_1^2 D_{i-1}^{k+1} - (h_1^2 - h_{-1}^2) D_i^{k+1}}{h_1(h_{-1}^2 - h_1 h_{-1})}$, $D_{rr} = \frac{2}{h_{-1} D_{i+1}^{k+1} - h_1 D_{i-1}^{k+1} + (h_1 - h_{-1}) D_i^{k+1}} \frac{h_{-1}(h_1 h_{-1} - h_{-1}^2)}{h_1(h_1 h_{-1} - h_{-1}^2)}$, $u_r = \frac{h_{-1}^2 u_{i+1}^{k+1} - h_1^2 u_{i-1}^{k+1} - (h_1^2 - h_{-1}^2) u_i^{k+1}}{h_1(h_{-1}^2 - h_1 h_{-1})}$, $h_{-1} = r_{i-1}^{k+1} - r_i^{k+1}$ and $h_1 = r_{i+1}^{k+1} - r_i^{k+1}$. The mesh moves by $r_i^{k+1} = r_i^k + u_i^{k+1} \tau$, where u_i^{k+1} is solved by the velocity equation.

Acknowledgements

This work is supported by the Mathematical Biosciences Institute and the National Science Foundation (Grant DMS 0931642), and by the Renmin University of China and the National Natural Science Foundation of China (Grant No. 11501568), and the International Postdoctoral Exchange Fellowship Program 2016 by the Office of China Postdoctoral Council.

Availability of data and materials

The dataset supporting the conclusions of this article is included within the article.

Authors' contributions

XL and AF developed and simulated the model, and wrote the final manuscript. Both authors read and approved the final manuscript.

Competing interests

The authors declare that they have no competing interests.

Publisher's Note

Springer Nature remains neutral with regard to jurisdictional claims in published maps and institutional affiliations.

Author details

¹Institute for Mathematical Sciences, Renmin University of China, 100872 Beijing, People's Republic of China. ²Mathematical Bioscience Institute & Department of Mathematics, Ohio State University, 43210 Columbus, OH, USA.

Received: 22 February 2017 Accepted: 11 July 2017

Published online: 19 July 2017

References

- Cheng X, Veverka V, Radhakrishnan A, Waters LC, Muskett FW, Morgan SH, et al. Human pd-1/b7-h1/cd274 protein. Sino Biological Inc. <http://www.sinobiological.com/PD-L1-B7-H1-CD274-Protein-g-533.html>. Accessed 2002.
- Shi L, Chen S, Yang L, Li Y. The role of pd-1 and pd-l1 in t-cell immune suppression in patients with hematological malignancies. *J Hematol Oncol*. 2013;6(74):10–118617568722674.
- Muppidi MR, George S. Immune checkpoint inhibitors in renal cell carcinoma. *J Targeted Ther Cancer*. 2015;4:47–52.
- Cooper ZA, Juneja VR, Sage PT, Frederick DT, Piris A, Mitra D, et al. Response to braf inhibition in melanoma is enhanced when combined with immune checkpoint blockade. *Cancer Immunol Res*. 2014;2(7):643–54.
- Wilmott JS, Long GV, Howle JR, Haydu LE, Sharma RN, Thompson JF, et al. Selective braf inhibitors induce marked t-cell infiltration into human metastatic melanoma. *Clin Cancer Res*. 2012;18(5):1386–94.
- He J, Hu Y, Hu M, Li B. Development of pd-1/pt-1 pathway in tumor immune microenvironment and treatment for non-small cell lung cancer. *Sci Rep*. 2015;5(13110):10–103813110.
- Ascierto PA, Kirkwood JM, Grob JJ, Simeone E, Grimaldi AM, Maio M, et al. The role of braf v600 mutation in melanoma. *J Transl Med*. 2012;10(85):1–9.
- Sanchez-Laorden B, Viros A, Girotti MR, Pedersen M, Saturno G, Zambon A, et al. Braf inhibitors induce metastasis in ras mutant or inhibitor-resistant melanoma cells by reactivating mek and erk signaling. *Sci Signal*. 2014;7(318):30.
- Menzies AM, Long GV. Recent advances in melanoma systemic therapy. braf inhibitors, ctla4 antibodies and beyond. *Eur J Cancer*. 2013;49(15):3229–241.
- Eroglu Z, Ribas A. Combination therapy with braf and mek inhibitors for melanoma: latest evidence and place in therapy. *Ther Adv Med Oncol*. 2016;8(1):48–56.
- Ott PA. Combined braf and mek inhibition in brafv600e mutant melanoma: a synergistic and potentially safe combination partner with immunotherapy. *Ann Transl Med*. 2015;3(20):313.
- Topalian SL, Sznol M, McDermott DF, Kluger HM, Carvajal RD, Sharfman WH, et al. Survival, durable tumor remission, and long-term safety in patients with advanced melanoma receiving nivolumab. *J Clin Oncol*. 2014;32(10):1020–30.
- Sugiura K, Sugiura M. Immune checkpoint blockade therapy: Merits and demerits. *J Clin Exp Dermatol Res*. 2016;7(372):10–4172215595541000372.
- Hu-Lieskovan S, Mok S, Moreno BH, Tsoi J, Faja LR, Goedert L, et al. Improved antitumor activity of immunotherapy with braf and mek inhibitors in brafv600e melanoma. *Sci Transl Med*. 2016;7(279):279–41.
- Kawakami Y, Yaguchi T, Sumimoto H, Kudo-Saito C, Iwata-Kajihara T, Nakamura S, et al. Improvement of cancer immunotherapy by combining molecular targeted therapy. *Front Oncol*. 2013;3(136):1–7.
- Devji T, Levine O, Neupane B, Beyene J, Xie F. Systemic therapy for previously untreated advanced braf-mutated melanoma: A systematic review and network meta-analysis of randomized clinical trials. *JAMA Oncol*. 3(3):366–73.
- Hargadon KM, Bishop JD, Brandt JP, Hand ZC, Ararso YT, Forrest OA. Melanoma-derived factors alter the maturation and activation of differentiated tissue-resident dendritic cells. *Immunol Cell Biol*. 2016;94(1):24–38.
- Ott PA, Henry T, Baranda SJ, Frleta D, Manches O, Bogunovic D, et al. Inhibition of both braf and mek in braf(v600e) mutant melanoma restores compromised dendritic cell (dc) function while having differential direct effects on dc properties. *Cancer Immunol Immunother*. 2013;62(4):811–22.
- Ilieva KM, Correa I, Josephs DH, Karagiannis P, Egbuniwe IU, Cafferkey MJ, et al. Effects of braf mutations and braf inhibition on immune responses to melanoma. *Mol Cancer Ther*. 2014;13(12):2769–83.
- Janco JMT, Lamichane P, Karyampudi L, Knutson KL. Tumor-infiltrating dendritic cells in cancer pathogenesis. *J Immunol*. 2015;194(7):2985–91.
- Ma Y, Shurin GV, Peiyuan Z, Shurin MR. Dendritic cells in the cancer microenvironment. *J Cancer*. 2013;4(1):36–44.
- Haabeth OAW, Tveita AA, Fauskanger M, Schjesvold F, Lorvik KB, Hofgaard PO, et al. How do cd4(+) t cells detect and eliminate tumor cells

- that either lack or express mhc class ii molecules? *Front Immunol.* 2014;5(174):1–13.
23. Kim HJ, Cantor H. Cd4 t-cell subsets and tumor immunity: the helpful and the not-so-helpful. *Cancer Immunol Res.* 2014;2(2):91–8.
 24. Thomas WD, Hersey P. Tnf-related apoptosis-inducing ligand (trail) induces apoptosis in fas ligand-resistant melanoma cells and mediates cd4 t cell killing of target cells. *J Immunol.* 1998;161(5):2195–200.
 25. Schattner EJ, Mascarenhas J, Bishop J, Yoo DH, Chadburn A, Crow M, et al. Cd4+ t-cell induction of fas-mediated apoptosis in burkitt's lymphoma b cells. *Blood.* 1996;88(4):1375–82.
 26. Martinez-Lostao L, Anel A, Pardo J. How do cytotoxic lymphocytes kill cancer cells? *Clin Cancer Res.* 2015;21(22):5047–56.
 27. Perrot CY, Javelaud D, Mauviel A. Insights into the transforming growth factor-beta signaling pathway in cutaneous melanoma. *Ann Dermatol.* 2013;25(2):135–44.
 28. Oelkrug C, Ramage JM. Enhancement of t cell recruitment and infiltration into tumours. *Clin Exp Immunol.* 2014;178(1):1–8.
 29. Jobe NP, Rösel D, Dvořánková B, Kodet O, Lacina L, Mateu R, et al. Simultaneous blocking of il-6 and il-8 is sufficient to fully inhibit caf-induced human melanoma cell invasiveness. *Histochem Cell Biol.* 2016;146(2):205–17.
 30. Whiteside TL. The role of regulatory t cells in cancer immunology. *Immunotargets Ther.* 2015;4:159–71.
 31. Umansky V, Blattner C, Gebhardt C, Utikal J. The role of myeloid-derived suppressor cells (mdsc) in cancer progression. *Vaccines.* 2016;4(36):1–16.
 32. Munn DH, Mellor AL. Ido in the tumor microenvironment: Inflammation, counter-regulation, and tolerance. *Trends in Immunology.* 2016;37(3):193–207.
 33. Sims GP, Rowe DC, Rietdijk ST, Herbst R, Coyle AJ. Hmgb1 and rage in inflammation and cancer. *Annu Rev Immunol.* 2010;28:367–88.
 34. Zandarashvili L, Sahu D, Lee K, Lee YS, Singh P, Rajarathnam K, et al. Real-time kinetics of high-mobility group box 1 (hmgb1) oxidation in extracellular fluids studied by in situ protein nmr spectroscopy. *J Biol Chem.* 2013;288(17):11621–7.
 35. Palucka J, Banchereau J. Cancer immunotherapy via dendritic cells. *Nat Rev Cancer.* 2012;12(4):265–77.
 36. Saenz R, Futalan D, Leutenetz L, Eekhout F, Fecteau JF, Sundelius S, et al. Tlr4-dependent activation of dendritic cells by an hmgb1-derived peptide adjuvant. *J Transl Med.* 2014;12(211):1–11.
 37. Chen D, Roda JM, Marsh CB, Eubank TD, Friedman A. Hypoxia inducible factors-mediated inhibition of cancer by gm-csf: a mathematical model. *Bull Math Biol.* 2012;74(11):2752–77.
 38. Eubank TD, Roberts RD, Khan M, Curry JM, Nuovo GJ, Kuppusamy P, et al. Granulocyte macrophage colony-stimulating factor inhibits breast cancer growth and metastasis by invoking an anti-angiogenic program in tumor-educated macrophages. *Cancer Res.* 2009;69(5):2133–40.
 39. Frederick DT, Piris A, Cogdill AP, Cooper ZA, Lezcano C, Ferrone CR, et al. Braf inhibition is associated with enhanced melanoma antigen expression and a more favorable tumor microenvironment in patients with metastatic melanoma. *Clin Cancer Res.* 2013;19(5):1225–31.
 40. Hao W, Rovin BH, Friedmann A. Mathematical model of renal interstitial fibrosis. *Proc Natl Acad Sci U S A.* 2014;111(39):14193–8.
 41. Condamine T, Gabrilovich DI. Molecular mechanisms regulating myeloid-derived suppressor cell differentiation and function. *Trends Immunol.* 2011;32(1):19–25.
 42. Cantelli G, Crosas-Molist E, Georgouli M, Sanz-Moreno V. Tgfb-induced transcription in cancer. *Semin Cancer Biol.* 2016;42:60–9.
 43. Mautea RL, Gordona SR, Mayere AT, McCrackena MN, Natarajane A, Ring NG, et al. Engineering high-affinity pd-1 variants for optimized immunotherapy and immuno-pet imaging. *Proc Natl Acad Sci USA.* 2015;112(47):6506–14.
 44. Hu-Lieskovan S, Mok S, Moreno BH, Tsoi J, Faja LR, Goedert L, et al. Improved antitumor activity of immunotherapy with braf and mek inhibitors in braf(v600e) melanoma. *Sci Transl Med.* 2015;7(279):1–11.
 45. D'Acunto B. *Computational Methods for PDE in Mechanics. Series on Advances in Mathematics for Applied Sciences-Vol.67.* Singapore: World Scientific; 2004.
 46. Marino S, Hogue I, Ray C, Kirschner D. A methodology for performing global uncertainty and sensitivity analysis in systems biology. *J Theor Biol.* 2008;254(1):178–96.
 47. Yin N, Ma W, Pei J, Ouyang Q, Tang C, Lai L. Synergistic and antagonistic drug combinations depend on network topology. *PLoS ONE.* 2014;9(4):93960.
 48. Jia J, Zhu F, Ma X, Cao ZW, Li YX, Chen YZ. Mechanisms of drug combinations: interaction and network perspectives. *Nat Rev Drug Discov.* 2009;8(2):111–28.
 49. Young ME. Estimation of diffusion coefficients of proteins. *Biotech Bioeng.* 1980;XXII:947–55.
 50. Shui YB, Wang X, Hu JS, Wang SP, Garcia CM, et al. Vascular endothelial growth factor expression and signaling in the lens. *Invest Ophthalmol Vis Sci.* 2003;44(9):3911–9.
 51. Liao KL, Bai XF, Friedman A. Mathematical modeling of interleukin-27 induction of anti-tumor t cells response. *PLoS ONE.* 2014;9(3):91844.
 52. PhosphoSitePlus/IL2(human). <http://www.phosphosite.org/proteinAction.action?id=14691&showAllSites=true>. Accessed 2003.
 53. Hamza T, Barnett JB, Li B. Interleukin 12 a key immunoregulatory cytokine in infection applications. *Int J Mol Sci.* 2010;11(3):789–806.
 54. Poniatowski LA, Wojdasiewicz P, Gasik R, Szukiewicz D. Transforming growth factor beta family: Insight into the role of growth factors in regulation of fracture healing biology and potential clinical applications. *Mediat Inflamm.* 2015;(Article ID 137823):1–17.
 55. Abcam/. Recombinant human il6 protein (ab9627). <http://www.abcam.com/recombinant-human-il6-protein-ab9627.html>.
 56. Keller ET, Wanagat J, Ershler WB. Stromelysin-1/matrix metalloproteinase-3 (mmp-3) expression accounts for invasive properties of human astrocytoma cell lines. *Front Biosci.* 1996;1(1):340–57.
 57. PhosphoSitePlus/IL10(human). <http://www.phosphosite.org/proteinAction.action?id=2473887&showAllSites=true>. Accessed 2003.
 58. Abcam/. Anti-pd1 antibody (ab89828). <http://www.abcam.com/pd1-antibody-ab89828.html>.
 59. Shah N, Iyer RM, Mair HJ, Choi DS, Tian H, Diodone R, et al. Improved human bioavailability of vemurafenib, a practically insoluble drug, using an amorphous polymer-stabilized solid dispersion prepared by a solvent-controlled coprecipitation process. *J Pharm Sci.* 2013;102(3):967–81.
 60. Steptoe RJ, Patel RK, Subbotin VM, Thomson AW. Comparative analysis of dendritic cell density and total number in commonly transplanted organs: morphometric estimation in normal mice. *Transpl Immunol.* 2000;8(1):49–56.
 61. Bergstresser PR, Fletcher CR, Streilein JW. Surface densities of langerhans cells in relation to rodent epidermal sites with special immunologic properties. *J Invest Dermatol.* 1980;74(2):77–88.
 62. Romani N, Clausen BE, Stoitzner P. Langerhans cells and more: langerin-expressing dendritic cell subsets in the skin. *Immunol Rev.* 2010;234(1):120–41.
 63. Dumortier H, van Mierlo GJD, Egan D, van Ewijk W, Toes REM, Offringa R, et al. Antigen presentation by an immature myeloid dendritic cell line does not cause ctl deletion in vivo, but generates cd8+ central memory-like t cells that can be rescued for full effector function. *J Immunol.* 2005;175(2):855–63.
 64. Ataera H, Hyde E, Price KM, Stoitzner P, Ronchese F. Murine melanoma-infiltrating dendritic cells are defective in antigen presenting function regardless of the presence of cd4cd25 regulatory t cells. *PLoS ONE.* 2011;6(3):17515.
 65. Hao W, Friedman A. The role of exosomes in pancreatic cancer microenvironment. *Bull Math Biol.* 2017;1–23. doi:10.1007/s11538-017-0254-9.
 66. Hao W, Schlesinger LS, Friedman A. Modeling granulomas in response to infection in the lung. *PLoS ONE.* 2016;11(3):0148738.
 67. Hussein MR. Tumour-associated macrophages and melanoma tumourigenesis: integrating the complexity. *Int J Exp Pathol.* 2006;87(3):163–76.
 68. Tian H, Shi G, Wang Q, Li Y, Yang Q, Li C, et al. A novel cancer vaccine with the ability to simultaneously produce anti-pd-1 antibody and gm-csf in cancer cells and enhance th1-biased antitumor immunity. *Signal Transduct Target Ther.* 2016;1(16025):10–1038201625.
 69. Li B, VanRoey M, Wang C, Chen TH, Korman A, Jooss K. Anti-programmed death-1 synergizes with granulocyte macrophage colony-stimulating factor-secreting tumor cell immunotherapy providing therapeutic benefit to mice with established tumors. *Clin Cancer Res.* 2009;15(5):1623–1634.

70. Ali OA, Lewin SA, Dranoff G, Mooney DJ. Vaccines combined with immune checkpoint antibodies promote cytotoxic t cell activity and tumor eradication. 2015. doi: 10.1158/2326-6066.CIR-14-0126.
71. Chun Y, Wang Y, Vo A, Liu H, Wang D, Gershenwald J, et al. Elevated interleukin-12 is a plasma marker of poor prognosis in stage iii melanoma patients. *Am Association for Cancer Res.* 2008;68(9):1.
72. Bankhead C. Aacr: Il-12 level may predict melanoma prognosis. *Medpage Today.* 2008;9177. <https://www.medpagetoday.com/meetingcoverage/aacr/9177>.
73. Kaminska B, Wesolowska A, Danilkiewicz M. Tgf beta signalling and its role in tumour pathogenesis. *Acta Biochim Pol.* 2005;52(2):329–37.
74. Kyrtsolis MC, Repa C, Dedoussis GV, Mouzaki A, Simeonidis A, Stamatelou M, et al. Serum transforming growth factor-beta 1 is related to the degree of immunoparesis in patients with multiple myeloma. *Med Oncol.* 1998;15(2):124–8.
75. Lo WC, Arsenescu V, Arsenescu RI, Friedman A. Inflammatory bowel disease: How effective is tnf-alpha suppression? *PLoS One.* 2016;11(11):0165782.
76. Ridker PM, Rifai N, Stampfer MJ, Hennekens CH. Plasma concentration of interleukin-6 and the risk of future myocardial infarction among apparently healthy men. *Clin Investig Rep.* 2000;101:1767–72.
77. Hojberg L, Bastholt L, Johansen JS, Christensen JI, Gehl J, Schmidt H. Serum interleukin-6 as a prognostic biomarker in patients with metastatic melanoma. *Melanoma Res.* 2012;22(4):287–93.
78. Mueller C, Braag SA, Martino AT, Tang Q, Campbell-Thompson M, Flotte T. The pros and cons of immunomodulatory il-10 gene therapy with recombinant aav in a cftr-/-dependent allergy mouse model. *Gene Therapy.* 2009;16:172–83.
79. Nemunaitis J, Fong T, Shabe P, Martineau D, Ando D. Comparison of serum interleukin-10 (il-10) levels between normal volunteers and patients with advanced melanoma. *Cancer Invest.* 2001;19(3):239–47.
80. Itakura E, Huang RR, Wen DR, Paul E, Wunsch PH, Cochran AJ. Il-10 expression by primary tumor cells correlates with melanoma progression from radial to vertical growth phase and development of metastatic competence. *Mod Pathol.* 2011;24(6):801–9.
81. Agata Y, Kawasaki A, Nishimura H, Ishida Y, Tsubat T, Yagita H, et al. Expression of the pd-1 antigen on the surface of stimulated mouse t and b lymphocytes. *Int Immunol.* 1996;8(5):765–72.
82. Cheng X, Veverka V, Radhakrishnan A, Waters LC, Muskett FW, Morgan SH, et al. Structure and interactions of the human programmed cell death 1 receptor. *J Biol Chem.* 2013;288(17):11771–85.
83. Lowther DE, Goods BA, Lucca LE, Lerner BA, Raddassi K, van Dijk D, et al. Pd-1 marks dysfunctional regulatory t cells in malignant gliomas. *JCI Insight.* 2016;1(5):85935.
84. Buttea MJ, Pena-Cruz V, Kima MJ, Freemanc GJ, Sharpe AH. Interaction of human pd-1 and b7-1. *Mol Immunol.* 2008;45(13):3567–72.
85. Schalper KA, Carvajal-Hausdorf D, McLaughlin J, Velcheti V, Chen L, Sanmamed M, et al. Clinical significance of pd-1 protein expression on tumor-associated macrophages in lung cancer. *J Immunother Cancer.* 2015;3(Suppl 2):415.
86. Lipson EJ, Sharfman WH, Drake CG, Wollner I, Taube JM, Anders RA, et al. Durable cancer regression off-treatment and effective reinduction therapy with an anti-pd-1 antibody. *Clin Cancer Res.* 2013;19(2):462–8.
87. Brahmer JR, Drake CG, Wollner I, Powderly JD, Picus J, Sharfman WH, et al. Phase i study of single-agent anti-programmed death-1 (mdx-1106) in refractory solid tumors: Safety, clinical activity, pharmacodynamics, and immunologic correlates. *J Clin Oncol.* 2010;28(19):3167–75.
88. Luke JJ, Ott PA. New developments in the treatment of metastatic melanoma - role of dabrafenib-trametinib combination therapy. *Drug Healthc Patient Saf.* 2014;6:77–88.
89. rey R Infante J, Fecher LA, Falhook GS, Nallapareddy S, Gordon MS, Becerra C, et al. Safety, pharmacokinetic, pharmacodynamic, and effi cacy data for the oral mek inhibitor trametinib: a phase 1 dose-escalation trial. *Lancet Oncol.* 2012;13(8):773–81.
90. Kima Y, Lawlerb S, Nowickib MO, Chioccab EA, Friedman A. A mathematical model for pattern formation of glioma cells outside the tumor spheroid core. *J Theor Biol.* 2009;260(3):359–71.
91. Mercapide J, Cicco RLD, Castresana JS, Klein-Szanto AJP. Stromelysin-1/matrix metalloproteinase-3 (mmp-3) expression accounts for invasive properties of human astrocytoma cell lines. *Int J Cancer.* 2003;106(5):676–82.

Submit your next manuscript to BioMed Central and we will help you at every step:

- We accept pre-submission inquiries
- Our selector tool helps you to find the most relevant journal
- We provide round the clock customer support
- Convenient online submission
- Thorough peer review
- Inclusion in PubMed and all major indexing services
- Maximum visibility for your research

Submit your manuscript at
www.biomedcentral.com/submit

